This article has been accepted for publication in a future issue of this journal, but has not been fully edited. Content may change prior to final publication. Citation information: DOI 10.1109/TPWRS.2017.2707564, IEEE Transactions on Power Systems

Chordal Relaxation Based ACOPF for Unbalanced Distribution Systems with DERs and Voltage Regulation Devices

Yikui Liu, *Student Member*, *IEEE*, Jie Li, *Member*, *IEEE*, Lei Wu, *Senior Member*, *IEEE*, Tom Ortmeyer, *Fellow*, *IEEE*

***Abstract*—In emerging distribution systems with a proliferation of distributed energy resources (DER) and flexible demand assets, operation characters of the unbalance network and voltage regulation devices need to be accurately addressed for ensuring the secure and economic operation. This paper focuses on the modeling and solution approach of AC optimal power flow (ACOPF) for unbalanced distribution systems with DERs and voltage regulation transformers (VRT). The ACOPF problem is formulated as a chordal relaxation based semidefinite programming (SDP) model, and a tighter convexification model of VRTs is proposed for mitigating solution inexactness. Analytical conditions are presented and proved to determine whether global optimal solution to the original ACOPF problem can be retrieved from solutions of the chordal relaxation based SDP model. Numerical studies on modified IEEE 34-bus and 8500-node systems show that the proposed approach presents a better computational performance as compared to rank relaxation based SDP approaches and general nonlinear solvers.**

***Index Terms*—Chordal relaxation, distribution ACOPF, SDP, unbalanced three-phase distribution system, voltage regulation.**

NOMENCLATURE

Indices:

d, g	Index of loads/DERs
m, n	Indices of buses
(n,m)	Index of line or ideal transformer connected with bus n and m
s	Index of static var compensators (SVC) and static synchronous compensators (STATCOM)
ϕ, ρ, ψ	Indices of phases

Sets and Vectors:

$\boldsymbol{B}$	Set of buses
$\boldsymbol{\mathcal{D}}$, $\boldsymbol{\mathcal{F}}$	Set of flexible loads/ constant power loads
$\mathbf{e}_n^{\phi}$	Standard basis vector of $\mathbb{R}^{3(N+K)\times 1}$ with the $(3n+1)^{th}$, $(3n+2)^{th}$, and $(3n+3)^{th}$ elements being "1" for phases a, b, and c, respectively. $\mathbb{R}$ is the set of real numbers
$\boldsymbol{e}^{\phi}$	Standard basis vector of $\mathbb{R}^{3\times 1}$, i.e., $[1\ 0\ 0]^T$ / $[0\ 1\ 0]^T$/$[0\ 0\ 1]^T$ for phase a/b/c
$\boldsymbol{\mathcal{G}}$, $\boldsymbol{\mathcal{R}}$	Set of conventional DERs/renewable DERs
$\boldsymbol{\mathcal{L}}$	Set of lines
$\boldsymbol{\mathcal{S}}$	Set of SVCs and STATCOMs
$\boldsymbol{\mathcal{T}}$	Set of ideal transformers
$\boldsymbol{\Psi}$	Set of phases, i.e., $\boldsymbol{\Psi}=\{a,b,c\}$
$\boldsymbol{\Omega}_n$	Set of buses that are connected to bus n
$\mathbf{0}$	Matrix/vector with all zeros

Variables:

$I_{(n,m)}^{\phi}$	Line current on phase ϕ of line $(n,m)\in\boldsymbol{\mathcal{L}}$
P_0^{ϕ}, Q_0^{ϕ}	Real/reactive power injection at phase ϕ of the distribution substation bus (indexed as 0)
P_d, Q_d	Real/reactive power withdraw of flexible load d
P_g, Q_g	Real/reactive power injection from DER g
P_n^{ϕ}, P_m^{ϕ}	Active power transmitted through phase ϕ of ideal transformer $(n,m)\in\boldsymbol{\mathcal{T}}$
Q_n^{ϕ}, Q_m^{ϕ}	Reactive power transmitted through phase ϕ of ideal transformer $(n,m)\in\boldsymbol{\mathcal{T}}$
Q_s	Reactive power injection of SVC/STATCOM s
$r_{n,m}$	Tap ratio of ideal transformer $(n,m)\in\boldsymbol{\mathcal{T}}$
V_n^{ϕ}	Complex voltage at phase ϕ of bus n
$\mathbf{V}$	Vector of complex voltage variables, i.e., $\mathbf{V}=[V_0^a\ \ V_0^b\ \ V_0^c\ \ldots V_{N+T}^a\ \ V_{N+T}^b\ \ V_{N+T}^c]^T$

Constants:

b_{d2}, b_{d1}, b_{d0}	Coefficients of benefit function for flexible load d
c_{g2}, c_{g1}, c_{g0}	Coefficients of cost/tariff function for DER g
N, K	Total number of buses/VRTs
PF	Power factor
P_d, Q_d	Real/reactive power of a fixed load $d\in\boldsymbol{\mathcal{F}}$
$\hat{\mathbf{V}}_0$	Given voltage values of the distribution substation bus, i.e., $\hat{\mathbf{V}}_0=[\hat{V}_0^a\ \ \hat{V}_0^b\ \ \hat{V}_0^c]^T$
S_g^{max}	Maximum apparent power limit of the invertor for renewable DER $g\in\boldsymbol{\mathcal{R}}$
^{min}, ^{max}	Lower/upper bound of a certain parameter

Symbols:

$diag(\cdot)$	Diagonal sub-matrix
$tr(\cdot)$	Trace
$rank(\cdot)$	Rank
$(\cdot)^T$	Transpose
$(\cdot)^*$	Conjugate
$(\cdot)^H$	Conjugate transpose
$\lvert\cdot\rvert$, $\lvert[\cdot]\rvert$	Magnitude/determinant

I. INTRODUCTION

Emerging distribution systems are envisioned to include a deeper penetration of distributed energy resources (DER) and flexible demand assets. DERs provide electricity locally in distribution systems, which could reduce real power losses, promote energy sustainability, enhance resiliency, and defer generation and transmission upgrades. However, they also present new challenges to distribution system operations.

This work was supported in part by the U.S. National Science Foundation grants PFI:BIC-1534035, CNS-1647135, and ECCS-1653179. The authors are with Electrical and Computer Engineering Department, Clarkson University, Potsdam, NY 13699 USA. (E-mail: yikliu, jieli, lwu, tortmeye@clarkson.edu).

This article has been accepted for publication in a future issue of this journal, but has not been fully edited. Content may change prior to final publication. Citation information: DOI 10.1109/TPWRS.2017.2707564, IEEE Transactions on Power Systems

Specifically, unlike traditional distribution systems with unidirectional power flows, a proliferation of DERs creates bidirectional power flows in emerging distribution systems and in turn their optimal dispatch is of crucial importance. In addition, with high resistance to reactance ratio, voltage magnitudes of distribution systems are also sensitive to real power injections of DERs, and a deeper penetration of DERs could cause voltage rise issues [1].

In order to address such challenges, AC optimal power flow (ACOPF) models and solution approaches are of crucial importance to the secure and economic operation of emerging distribution systems. Indeed, it has been recommended by the National Academies of Sciences that ACOPF models should be developed and tested with optimization algorithms, for reducing the risk of voltage collapse and enabling the effective utilization of existing line capacities [2].

ACOPF problem of distribution systems is nonlinear and nonconvex because of the quadratic relationship among voltages and real/reactive power injections of three phases at individual buses. Early works on ACOPF explored different mathematical models including linear programming (LP), quadratically constrained quadratic programming (QCQP), and nonlinear programming (NLP), as well as various solution algorithms such as Lagrange relaxation, interior point method, and heuristic approaches. General purpose NLP solvers have also been applied to solve ACOPF problems. Among them, LP based models present the best computational performance in terms that the global optimal solution can be effectively obtained, even for large-scale systems; however, LP based models by approximating AC power flows inevitably contain considerable errors, especially for distribution systems with high R/X ratios and untransposed line segments. On the other hand, QCQP and NLP based models can accurately simulate the nonlinear relationship among voltages and real/reactive power injections of three phases at individual buses in the distribution system; however, computational efficiency and solution quality remain to be major concerns, especially when applied to large-scale distribution systems [2].

Recently, convex relaxation techniques are explored for obtaining global optimal solutions to the ACOPF problem of the transmission network with a high computational efficiency. Semidefinite relaxation was first introduced in power system applications by X. Bai et al. in [3]. A well-cited pioneering paper [4] built up the theoretical basis for applying semidefinite relaxation to the ACOPF problem. In the ACOPF problem, the semidefinite relaxation technique is referred to as "rank relaxation" [4]-[5], which explicitly indicates that the rank constraint has been removed in the convexified ACOPF model. In addition, the chordal relaxation technique was introduced by R.A. Jabr in [6]-[7], and applied to large-scale transmission network ACOPF problems in [8] for improving the computational performance. In [9]-[10], ACOPF problem of the transmission network was formulated as a polynomial optimization problem and solved by a hierarchy of moment relaxation based semidefinite programming (SDP) models. Although high-order moment relaxation is tighter than rank relaxation, the computational burden easily becomes intractable which inspired a sparse moment relaxation approach for improving the computational performance [10]. However, above mentioned works all targeted at transmission systems, in which three phases are balanced.

Convex relaxation techniques have also been applied for solving distribution ACOPF problems. ACOPF of balanced radial distribution networks was modeled as a second-order conic programming (SOCP) problem [11], which was solved via interior point method in polynomial time. The SOCP formulation in [11] was further extended to meshed networks in [12]. Reference [13] proposed a branch flow model and a conic relaxation technique for ACOPF of radial distribution systems, which can guarantee solution exactness only if load over-satisfaction is allowed. Reference [14] formulated ACOPF of balanced distribution systems as a rank relaxation based SDP problem, and presented similar load over-satisfaction condition for guaranteeing solution exactness. Pareto-front of the injection region of electricity networks was studied in [15], in order to obtain global optimal solutions to ACOPF for radial topology.

However, existing studies [11]-[15] exclusively neglect the inherent unbalance in network topology, which is common in low-voltage distribution networks with unbalanced three-phase loads, untransposed line segments, and single-/two-phase laterals. Different from balanced systems, coupling between three-phase currents cannot be offset in unbalanced distribution systems, and in turn solutions to balanced ACOPF fail to provide insightful operation instructions. Thus, unbalanced ACOPF models and solution approaches are in urgent need. Recently, ACOPF of unbalanced distribution systems was formulated as a rank-relaxed SDP model in [16], which was solved via the alternating direction method of multipliers (ADMM) algorithm. Reference [17] extended the branch flow model to three-phase systems and solved the problem by the ADMM algorithm. In addition, our previous work [18] applied the moment relaxation approach to the ACOPF problem of unbalanced distribution system, for deriving distribution locational marginal prices.

Bus voltage profile is also a critical concern commonly faced by distribution system operators. Several technologies, such as voltage regulation transformers (VRT), static var compensators (SVC), static synchronous compensators (STATCOM), and shunt capacitor banks, could help maintain voltage levels of load buses within an acceptable range. References [19]-[20] formulated ACOPF of unbalanced distribution systems as a rank-relaxed SDP model while considering VRTs. However, it is observed that solutions in [19]-[20] are usually of high rank and infeasible to the original ACOPF. The main reason is that a VRT separates the distribution system into two sub-networks, while voltage phase angle difference between primary and secondary buses of a VRT is not properly constrained in the rank-relaxed SDP model [19]. An alternative VRT model to mitigate solution inexactness was proposed in [20], by directly connecting primary and secondary buses of a VRT via a pseudo branch. However, admittance values of pseudo branches are system-specific, which needs to be tuned carefully for deriving a

This article has been accepted for publication in a future issue of this journal, but has not been fully edited. Content may change prior to final publication. Citation information: DOI 10.1109/TPWRS.2017.2707564, IEEE Transactions on Power Systems

proper rank one solution. That is, if the admittance value is too small, the derived solution will be similar to the one without pseudo branch and in turn still inexact. While a large admittance would induce significant power flow on the pseudo branch, and the solution quality will be significantly compromised.

From existing literature we notice that: (i) prior convex relaxation based models for ACOPF problems, such as the rank relaxation, moment relaxation, and chordal relaxation based SDP models as well as the SOCP models, mainly target at three-phase balanced transmission and/or distribution systems; and (ii) assets in distribution systems, such as VRTs, are not accurately modelled and properly integrated. However, distribution systems, especially the low voltage distribution networks, are characterized with highly unbalanced network configurations and a wide variety of assets, which invalid the balanced models in practical applications.

This paper focuses on the ACOPF problem of unbalanced radial distribution systems with voltage regulation devices, including VRTs, SVCs, STATCOMs, and shunt capacitor banks. Two types of DERs are studied, in which conventional DERs are directly connected to the AC distribution network while renewable DERs such as photovoltaics are connected via inverters. The unbalanced ACOPF problem determines the optimal operation of DERs, flexible demand assets, and voltage regulation devices, in order to minimize the total operation cost. Structure of the unbalanced ACOPF problem is mapped into a chordal graph, and the unbalanced ACOPF problem is formulated as a chordal relaxation based SDP model [7], [21]. Additionally, a tighter convexification model of VRTs is introduced for mitigating solution inexactness. Case studies illustrate computational efficiency of the proposed approach as compared to rank relaxation based SDP approaches and general NLP solvers.

Major contributions of this paper include:

1) The proposed unbalanced ACOPF model accurately simulates operational characters of various assets in distribution systems, including conventional DERs, inverter interfaced renewable DERs, flexible loads, fixed loads, and various voltage regulation devices.
2) The unbalanced ACOPF problem is formulated as a chordal relaxation based SDP model by exploring problem structure, which improves the computational performance as compared to rank relaxation based SDP approaches and those directly solved by general NLP solvers.
3) A tighter convexification model for VRTs is explored to mitigate solution inexactness. Analytical conditions are presented and proved to determine whether global optimal solution to the original ACOPF problem can be retrieved from solutions of the chordal relaxation based SDP model.

The rest of the paper is organized as follows. Device models and the unbalanced ACOPF problem are presented in Section II. The chordal relaxation based SDP model of unbalanced ACOPF and a tighter convexification formulation of VRTs are discussed in Section III. Numerical case studies are presented in Section IV, and the conclusions are drawn in Section V.

II. ACOPF for Unbalanced Distribution Network

Unbalanced radial wye-connected distribution systems with three-conductor grounded or four-conductor multi-grounded neutral are considered. In such systems, impedance matrices of lines and three-phase wye-wye solidly grounded VRTs can be written as 3×3 phase frame matrices. Admittance matrix of line $(n,m) \in \boldsymbol{\mathcal{L}}$ can be simulated as a 3×3 phase frame complex matrix $\boldsymbol{Y}_{(n,m)}$. For single- and two- phase lines, elements corresponding to missing phases in $\boldsymbol{Y}_{(n,m)}$ are zeroes.

A. Modeling of Loads and DERs

Both fixed loads, including constant power loads (CPL) and constant impedance loads (CIL), and flexible loads are studied. A CPL $d \in \boldsymbol{\mathcal{F}}$ is modeled via fixed real and reactive power demands P_d and Q_d. A CIL is modeled by a 3×3 impedance matrix shunted at the connecting bus, which can be combined into impedance matrix of the distribution system.

Equation (1) represents the benefit function of a flexible load $d \in \boldsymbol{\mathcal{D}}$, which measures the monetary benefit in terms of satisfaction or happiness that a consumer achieves by consuming electricity. Intuitively, benefit function denotes the consumer's willingness to pay for the electric energy consumption [22]. Benefit functions can be modeled as quadratic, logarithmic, or exponential functions [22]. In this paper, the quadratic function (1) is considered, in which b_{d2}, b_{d1}, and b_{d0} are quadratic, linear, and constant parameters. A flexible load d can adjust its real and reactive power ouputs within specified regions (2), which are also restricted by the power factor limit (3). The power factor limit (3) represents the requirement for reducing the non-productive reactive power from the utility.

$$B_d(P_d) = b_{d2} \cdot P_d^2 + b_{d1} \cdot P_d + b_{d0} \tag{1}$$

$$P_d^{min} \le P_d \le P_d^{max}; \qquad Q_d^{min} \le Q_d \le Q_d^{max} \tag{2}$$

$$\frac{PF_d^{min}}{\sqrt{1-\left(PF_d^{min}\right)^2}} Q_d \le P_d \le \frac{PF_d^{max}}{\sqrt{1-\left(PF_d^{max}\right)^2}} Q_d \tag{3}$$

Both conventional DERs (e.g., diesel and natural gas generator) and renewable DERs (e.g., wind and photovoltaics) are considered. Operation cost of a conventional DER $g \in \boldsymbol{\mathcal{G}}$ is represented as in (4). Real/reactive power limits and power factor limit are shown as in (5)-(6), respectively. The power factor limit (6) represents active power and reactive power boundaries within which the conventional DER can operate safely.

$$C_g\left(P_g\right) = c_{g2} \cdot P_g^2 + c_{g1} \cdot P_g + c_{g0} \tag{4}$$

$$P_g^{min} \le P_g \le P_g^{max}; \qquad Q_g^{min} \le Q_g \le Q_g^{max} \tag{5}$$

$$\frac{PF_g^{min}}{\sqrt{1-\left(PF_g^{min}\right)^2}} Q_g \le P_g \le \frac{PF_g^{max}}{\sqrt{1-\left(PF_g^{max}\right)^2}} Q_g \tag{6}$$

Renewable DERs are commonly connected to the AC distribution network via inverters. The energy feed-in tariff function of a renewable DER $g \in \boldsymbol{\mathcal{R}}$ is represented as in (7), where parameter η_g represents inverter power loss factor. In current distribution systems, instead of directly owning renewable DERs, it is a common practice that utilities purchase electricity from renewable DER owners (such as

This article has been accepted for publication in a future issue of this journal, but has not been fully edited. Content may change prior to final publication. Citation information: DOI 10.1109/TPWRS.2017.2707564, IEEE Transactions on Power Systems

third parties or residential customers) through power purchase agreements (PPA) [23]. PPAs usually provide long-term fixed prices (i.e., feed-in tariff) to renewable DER owners for selling their excessive electricity. Real and reactive power outputs of a renewable DER g are constrained by real power limit (8), power factor limt (9), and inveter capacity limit (10).

$$C_g(P_g) = c_{g1} \cdot \left[\left(1+\eta_g\right) \cdot P_g\right] \tag{7}$$

$$P_g^{min} \le P_g \le P_g^{max} \tag{8}$$

$$\frac{PF_g^{min}}{\sqrt{1-\left(PF_g^{min}\right)^2}} Q_g \le P_g \le \frac{PF_g^{max}}{\sqrt{1-\left(PF_g^{max}\right)^2}} Q_g \tag{9}$$

$$P_g^2 + Q_g^2 \le \left(S_g^{max}\right)^2 \tag{10}$$

B. Modeling of Static Capacitor Banks, SVCs, and STATCOMs

Two types of reactive power compensation devices are studied. A static capacitor bank provides specific capacitance shunted at a bus, which can be modeled via a 3×3 impedance matrix and combined into admittance matrix of the distribution network. SVCs and STATCOMs can inject or withdraw reactive power at connecting buses while not involving real power, which is modeled as in (11).

$$Q_s^{min} \le Q_s \le Q_s^{max} \tag{11}$$

C. Modeling of VRTs

A VRT is modeled as an ideal transformer in series with an impedance [20], as shown in Fig. 1. The primary side of the ideal transformer is connected at bus n, and the secondary side is connected at a virtual bus m. The equivalent circuit is based on three assumptions: (i) exciting current is ignored; (ii) with a nominal tap ratio, winding resistance and leakage reactance referred to the secondary side are constants; and (iii) tap ratio is considered as a continuous decision variable to keep ACOPF as a differentiable NLP problem. In addition, three-phase tap ratio variables for a VRT are considered to be identical [24].

An ideal transformer $(n,m) \in \boldsymbol{\mathcal{T}}$ can be modeled as in (12)-(13). Constraint (12) indicates that VRTs only change voltage magnitudes but not voltage phase angles of secondary buses. Furthermore, an ideal transformer separates the distribution system into two parts, while P_n^ϕ, P_m^ϕ and Q_n^ϕ, Q_m^ϕ represent the real and reactive powers transmitted through the ideal transformer. That is, P_n^ϕ and Q_n^ϕ is regarded as a pseudo load at the primary bus, while P_m^ϕ and Q_m^ϕ is treated as a pseudo generation source at the secondary bus. Constraint (13) ensures that the active and reactive power inflows are equal to the outflows through an ideal transformer.

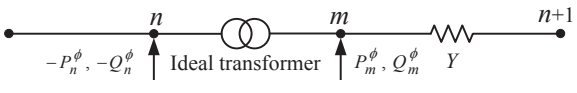

Fig. 1 Equivalent circuit of a voltage regulation transformer

$$r_{n,m} \cdot V_n^\phi = V_m^\phi; \quad r_{n,m}^{min} \le r_{n,m} \le r_{n,m}^{max} \tag{12}$$

$$P_n^\phi = P_m^\phi; \quad Q_n^\phi = Q_m^\phi \tag{13}$$

D. ACOPF of Unbalanced Three-phase Distribution Systems

For an N-node distribution system (including the distribution substation bus indexed as 0) with K VRTs, the equivalent system by substituting VRTs via circuits in Fig. 1 includes $(N+K)$ buses, i.e., N original buses and K virtual buses. In turn, the system three-phase nodal admittance matrix $\mathbf{Y} \in \mathbb{C}^{3(N+K)\times 3(N+K)}$ can be constructed according to the distribution network topology and 3×3 phase frame matrices of individual assets. $Y_{n,m}^{\phi,\rho}$ is an element of $\mathbf{Y}$ corresponding to phase ϕ of bus n and phase ρ of bus m.

The total complex power withdrawn from CILs, capacitor banks, and adjacent lines at phase ϕ of bus n can be calculated via V_n^ϕ multiplying the conjugate of their total current withdraw $\left(\sum_{\rho\in\boldsymbol{\Psi}} Y_{n,n}^{\phi,\rho} \cdot V_n^\rho + \sum_{m\in\boldsymbol{\Omega}_n}\sum_{\rho\in\boldsymbol{\Psi}} Y_{n,m}^{\phi,\rho} \cdot V_m^\rho\right)^*$. It can be further represented via a compact matrix form as in (14), where $\boldsymbol{\Phi}_{P,n}^\phi$ and $\boldsymbol{\Phi}_{Q,n}^\phi$ are defined in (15)-(16). The derivation of $\boldsymbol{\Phi}_{P,n}^\phi$ and $\boldsymbol{\Phi}_{Q,n}^\phi$ can be referred to [14]. Thus, real and reactive power balances at phase ϕ of bus n are presented via (17)-(18), where $\boldsymbol{\mathcal{F}}_n^\phi$, $\boldsymbol{\mathcal{G}}_n^\phi$, $\boldsymbol{\mathcal{R}}_n^\phi$, $\boldsymbol{\mathcal{D}}_n^\phi$, and $\boldsymbol{\mathcal{S}}_n^\phi$ are sets of CPLs, conventional DERs, renewable DERs, flexible loads, and SVCs/STATCOMs connected at phase ϕ of bus n, respectively. Λ_n is defined in (19) to represent the connecting topology of VRTs and the substation bus.

$$V_n^\phi \cdot \left(\sum_{\rho\in\boldsymbol{\Psi}} Y_{n,n}^{\phi,\rho} \cdot V_n^\rho + \sum_{m\in\boldsymbol{\Omega}_n}\sum_{\rho\in\boldsymbol{\Psi}} Y_{n,m}^{\phi,\rho} \cdot V_m^\rho\right)^* = tr\left(\boldsymbol{\Phi}_{P,n}^\phi \cdot \mathbf{V}\cdot\mathbf{V}^H\right) + j\cdot tr\left(\boldsymbol{\Phi}_{Q,n}^\phi \cdot \mathbf{V}\cdot\mathbf{V}^H\right) \tag{14}$$

$$\boldsymbol{\Phi}_{P,n}^\phi = \frac{1}{2}\left(\mathbf{Y}_n^\phi + \left(\mathbf{Y}_n^\phi\right)^H\right); \quad \boldsymbol{\Phi}_{Q,n}^\phi = \frac{j}{2}\left(\mathbf{Y}_n^\phi - \left(\mathbf{Y}_n^\phi\right)^H\right) \tag{15}$$

$$\mathbf{Y}_n^\phi = \mathbf{e}_n^\phi \cdot \left(\mathbf{e}_n^\phi\right)^T \cdot \mathbf{Y} \tag{16}$$

$$tr\left(\boldsymbol{\Phi}_{P,n}^\phi \cdot \mathbf{V}\cdot\mathbf{V}^H\right) = \sum_{g\in\boldsymbol{\mathcal{G}}_n^\phi\cup\boldsymbol{\mathcal{R}}_n^\phi} P_g - \sum_{d\in\boldsymbol{\mathcal{D}}_n^\phi\cup\boldsymbol{\mathcal{F}}_n^\phi} P_d + \Lambda_n \cdot P_n^\phi \tag{17}$$

$$tr\left(\boldsymbol{\Phi}_{Q,n}^\phi \cdot \mathbf{V}\cdot\mathbf{V}^H\right) = \sum_{g\in\boldsymbol{\mathcal{G}}_n^\phi\cup\boldsymbol{\mathcal{R}}_n^\phi} Q_g - \sum_{d\in\boldsymbol{\mathcal{D}}_n^\phi\cup\boldsymbol{\mathcal{F}}_n^\phi} Q_d + \sum_{s\in\boldsymbol{\mathcal{S}}_n^\phi} Q_s + \Lambda_n \cdot Q_n^\phi \tag{18}$$

$$\Lambda_n = \begin{cases} -1 & if\ (n,m)\in\boldsymbol{\mathcal{T}} \\ 1 & if\ (m,n)\in\boldsymbol{\mathcal{T}}\ \ or\ n=0 \\ 0 & otherwise \end{cases} \tag{19}$$

Given electricity price c_0 of all three phases at the distribution substation bus, ACOPF for unbalanced three-phase distribution systems can be formulated as a nonconvex QCQP problem (20), where ***.

$$\min_{\substack{\mathbf{V},P_d,Q_d,P_g,Q_g,\\ Q_s,r_{n,m},P_n^\phi,Q_n^\phi}} \left\{\begin{array}{l} \sum_{\phi\in\boldsymbol{\Psi}} c_0 \cdot P_0^\phi + \sum_{g\in\boldsymbol{\mathcal{G}}\cup\boldsymbol{\mathcal{R}}} C_g\left(P_g\right) \\ \quad - \sum_{d\in\boldsymbol{\mathcal{D}}} B_d(P_d) \end{array}\right\} \tag{20a}$$

$$\left(\left|V_n^\phi\right|^{min}\right)^2 \le tr\left(\mathbf{e}_n^\phi \cdot \left(\mathbf{e}_n^\phi\right)^T \cdot \mathbf{V}\cdot\mathbf{V}^H\right) \le \left(\left|V_n^\phi\right|^{max}\right)^2 \tag{20b}$$

$$tr\left(\boldsymbol{\Phi}_{I,(n,m)}^\phi \cdot \mathbf{V}\cdot\mathbf{V}^H\right) \le \left(\left|I_{(n,m)}^\phi\right|^{max}\right)^2; \quad (n,m)\in\boldsymbol{\mathcal{L}} \tag{20c}$$

$$[V_0^a,\ V_0^b,\ V_0^c]^T = \widehat{\mathbf{V}}_0 \tag{20d}$$

Subject to (2)-(3), (5)-(6), (8)-(13), and (17)-(18) (20e)

$$\boldsymbol{\Phi}_{I,(n,m)}^\phi = \boldsymbol{\mathcal{B}}^H \cdot \boldsymbol{e}^\phi \cdot \left(\boldsymbol{e}^\phi\right)^T \cdot \boldsymbol{\mathcal{B}} \tag{21}$$

$$\boldsymbol{\mathcal{B}} = \left[\mathbf{0}_{3\times 3\cdot n} \quad \boldsymbol{Y}_{(n,m)} \quad \mathbf{0}_{3\times 3\cdot(m-n-1)} \quad -\boldsymbol{Y}_{(n,m)} \quad \mathbf{0}_{3\times 3\cdot(N-m-1)}\right] \tag{22}$$

Objective function (20a) minimizes the total system operation cost, including the electricity purchase cost from the

This article has been accepted for publication in a future issue of this journal, but has not been fully edited. Content may change prior to final publication. Citation information: DOI 10.1109/TPWRS.2017.2707564, IEEE Transactions on Power Systems

main grid at the substation bus, the electricity production cost from local conventional DERs and renewable DERs within the distribution network, and the benefit from flexible loads. Constraint (20b) is the bus voltage magnitude limit, where $\left|V_n^{\phi}\right|^2 = V_n^{\phi} \cdot \left(V_n^{\phi}\right)^*$ is represented via a compact matrix form $tr\left(\mathbf{e}_n^{\phi} \cdot \left(\mathbf{e}_n^{\phi}\right)^T \cdot \mathbf{V} \cdot \mathbf{V}^H\right)$. Constraint (20c) represents the line current limit where $\mathbf{\Phi}_{I,(n,m)}^{\phi}$ and $\boldsymbol{\mathcal{B}}$ are defined as in (21)-(22) for $n < m$. Line current limit, rather than apparent power limit or active power limit, is considered due to the fact that line current measurements are deployed more widely in distribution systems than line power flow measurements. That is, distribution system operators usually monitor line currents instead of line power flow quantities in practice. Constraint (20d) sets voltages of the distribution substation bus.

III. Chordal Relaxation Based SDP Model for ACOPF

A. Graph Representation of the ACOPF Problem

In this paper, structure of the unbalanced ACOPF problem is mapped into a graph [25]. That is, in the graph of the ACOPF problem (20), each node represents a variable V_n^{ϕ}, while two nodes V_n^{ϕ} and V_m^{ρ} are connected via an edge if and only if $V_n^{\phi} \cdot \left(V_m^{\rho}\right)^*$ is involved in the ACOPF problem (20).

In the unbalanced ACOPF problem, subgraphs corresponding to phase voltages of two adjacent buses are shown in Fig. 2. Fig. 2(a)-2(c) show subgraphs of two adjacent three-, two-, and single- phase buses that are connected via a distribution line, while Fig. 2(d) shows a subgraph of two adjacent three-phase buses that are connected via an ideal transformer. The graph of the entire ACOPF problem can be constructed by connecting sub-structures in Fig. 2 successively according to the network topology. As $V_n^{a,b,c} \cdot \left(V_m^{a,b,c}\right)^*$ for $(n,m) \in \boldsymbol{\mathcal{T}}$ do not exist in (20), nodes $V_n^{a,b,c}$ and $V_m^{a,b,c}$ are not directly connected as shown in Fig. 2(d). That is, an ideal transformer will split the graph of the entire ACOPF problem into two separated sub-graphs.

The following observations are derived according to the graph of the unbalanced ACOPF problem (20). An illustrative example is provided in Appendix A to describe how the proposed ACOPF problem can be mapped into a chordal graph.

i) Although network topology of an unbalanced three-phase distribution system is radial, the graph of the ACOPF problem (20) is strongly meshed, as shown in Fig. 2(a). However, ACOPF approaches and conclusions for balanced distribution systems in [26] require the graph of ACOPF problems, instead of the system network topology, to be acyclic (i.e., radial), and in turn are not applicable to the unbalanced ACOPF problem (20).

ii) In graph theory, a cycle is a sequence of nodes starting and ending at the same node, with each two consecutive nodes in the sequence connected by an edge. A minimal cycle is defined as the smallest cycle that does not contain other cycles. A graph is called chordal if all minimal cycles in the graph include at most 3 nodes. Indeed, the graph of the ACOPF problem (20) is chordal.

iii) In graph theory, a *k*-clique is defined as a *k*-node complete subgraph in which each node is connected to all other (*k-1*) nodes. A maximal *k*-clique refers to a *k*-clique that is not contained in any other higher order cliques. Indeed, the graph of the ACOPF problem (20) is constituted of maximal 6-, 4-, and 2- cliques corresponding to three-, two-, and single- phase lines. $\boldsymbol{\mathcal{C}}$ represents the set of maximal cliques in the graph.

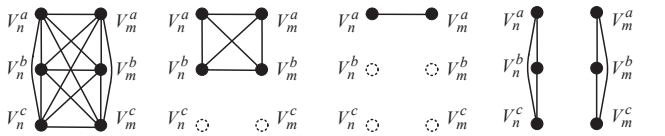

Fig. 2 Subgraphs corresponding to phase voltages of two adjacent buses

B. Chordal Relaxation Based SDP Model

In order to build the chordal relaxation based SDP model, new variables $\mathrm{W}_{n,m}^{\phi,\rho}$ are introduced to substitute nonlinear terms $V_n^{\phi} \cdot \left(V_m^{\rho}\right)^*$ in the ACOPF problem (20). For the sake of discussion, the variable substitution is denoted as "⇒", which substitutes $V_n^{\phi} \cdot \left(V_m^{\rho}\right)^*$ with variable $\mathrm{W}_{n,m}^{\phi,\rho}$ when corresponding $V_n^{\phi} \cdot \left(V_m^{\rho}\right)^*$ appears in (20) and zeros when $V_n^{\phi} \cdot \left(V_m^{\rho}\right)^*$ does not appear in (20). In turn, $\mathbf{W}$ is a $3 \cdot (N+K)$ by $3 \cdot (N+K)$ square matrix, which is constructed by $\mathbf{V} \cdot (\mathbf{V})^H \Rightarrow \mathbf{W}$. Similarly, $\mathbf{W}_c$ is defined for each maximal clique $c \in \boldsymbol{\mathcal{C}}$ in the graph, while the dimension of $\mathbf{W}_c$ can be 6×6, 4×4, or 2×2 corresponding to maximal 6-, 4-, and 2- cliques in Fig 2 (a)-(c). In addition, as maximal cliques are complete subgraphs, $\mathbf{W}_c$ does not contain zeros. An illustrative example is provided in Appendix B to further demonstrate the chordal relaxation approach and how to separate the $\mathbf{W}$ matrix into several sub-matrices $\mathbf{W}_c$.

As the graph of the ACOPF problem (20) is chordal and each $\mathbf{W}_c$ corresponds to a distribution line, the original ACOPF problem (20) can be reformulated as a chordal relaxation based SDP model (23). The objective function (23a) is represented as an epigraph form, while Schur's component forms are defined in (23b)-(23d). Constraints (23e)-(23f) correspond to real and reactive power balance constraints (17)-(18) for each phase at each bus. Constraint (23g) is a Schur's component form of the inverter capacity limit (10). Constraint (23h) is the voltage limit corresponding to (20b). Constraint (23i) is the line current limit corresponding to (20c) The given distribution substation bus voltages (20d) are expressed in the matrix form (23j). Constraint (23k) requires variable matrices $\mathbf{W}_c$ to be positive semidefinite. Constraints (23l)-(23m) are primary and secondary bus voltage constraints of an ideal transformer corresponding to (12). $\mathbf{W}_{n,m}$ is defined as $\begin{bmatrix} \mathrm{W}_{n,m}^{a,a} & \mathrm{W}_{n,m}^{a,b} & \mathrm{W}_{n,m}^{a,c} \\ \mathrm{W}_{n,m}^{b,a} & \mathrm{W}_{n,m}^{b,b} & \mathrm{W}_{n,m}^{b,c} \\ \mathrm{W}_{n,m}^{c,a} & \mathrm{W}_{n,m}^{c,b} & \mathrm{W}_{n,m}^{c,c} \end{bmatrix}$.

This article has been accepted for publication in a future issue of this journal, but has not been fully edited. Content may change prior to final publication. Citation information: DOI 10.1109/TPWRS.2017.2707564, IEEE Transactions on Power Systems

$$min_{\mathbf{W}_c,\beta_g,\vartheta_d,P_g,Q_g,P_d,Q_d,Q_s,r_{n,m},P_n^\phi,Q_n^\phi}\left\{\sum_{\phi\in\boldsymbol{\Psi}} c_0\cdot P_0^\phi+\sum_{g\in\boldsymbol{\mathcal{G}}\cup\boldsymbol{\mathcal{R}}}\beta_g-\sum_{d\in\boldsymbol{\mathcal{D}}}\vartheta_d\right\} \quad (23a)$$

$$\begin{bmatrix}\beta_g-c_{g1}\cdot P_g-c_{g0} & -\sqrt{c_{g2}}\cdot P_g\\ -\sqrt{c_{g2}}\cdot P_g & 1\end{bmatrix}\succcurlyeq 0;\quad g\in\boldsymbol{\mathcal{G}} \quad (23b)$$

$$\beta_g=c_{g1}\cdot\left[\left(1+\eta_g\right)\cdot P_g\right];\quad g\in\boldsymbol{\mathcal{R}} \quad (23c)$$

$$\begin{bmatrix}b_{d1}\cdot P_d+b_{d,0}-\vartheta_d & \sqrt{-b_{d2}}\cdot P_d\\ \sqrt{-b_{d2}}\cdot P_d & 1\end{bmatrix}\succcurlyeq 0;\quad d\in\boldsymbol{\mathcal{D}} \quad (23d)$$

$$tr\left(\boldsymbol{\Phi}_{P,n}^\phi\cdot\mathbf{W}\right)=\sum_{g\in\boldsymbol{\mathcal{G}}_n^\phi\cup\boldsymbol{\mathcal{R}}_n^\phi}P_g-\sum_{d\in\boldsymbol{\mathcal{D}}_n^\phi\cup\boldsymbol{\mathcal{F}}_n^\phi}P_d+\Lambda_n\cdot P_n^\phi \quad (23e)$$

$$tr\left(\boldsymbol{\Phi}_{Q,n}^\phi\cdot\mathbf{W}\right)=\sum_{g\in\boldsymbol{\mathcal{G}}_n^\phi\cup\boldsymbol{\mathcal{R}}_n^\phi}Q_g-\sum_{d\in\boldsymbol{\mathcal{D}}_n^\phi\cup\boldsymbol{\mathcal{F}}_n^\phi}Q_d+\sum_{s\in\boldsymbol{\mathcal{S}}_n^\phi}Q_s+\Lambda_n\cdot Q_n^\phi \quad (23f)$$

$$\begin{bmatrix}\left(S_g^{max}\right)^2 & P_g & Q_g\\ P_g & 1 & 0\\ Q_g & 0 & 1\end{bmatrix}\succcurlyeq 0;\quad g\in\boldsymbol{\mathcal{R}} \quad (23g)$$

$$\left(\left|V_n^\phi\right|^{min}\right)^2\le tr\left(\mathbf{e}_n^\phi\cdot\left(\mathbf{e}_n^\phi\right)^T\cdot\mathbf{W}\right)\le\left(\left|V_n^\phi\right|^{max}\right)^2 \quad (23h)$$

$$tr\left(\boldsymbol{\Phi}_{I,(n,m)}^\phi\cdot\mathbf{W}\right)\le\left(\left|I_{(n,m)}^\phi\right|^{max}\right)^2;\quad (n,m)\in\boldsymbol{\mathcal{L}} \quad (23i)$$

$$\mathbf{W}_0=\begin{bmatrix}\mathrm{W}_{0,0}^{a,a} & \mathrm{W}_{0,0}^{a,b} & \mathrm{W}_{0,0}^{a,c}\\ \mathrm{W}_{0,0}^{b,a} & \mathrm{W}_{0,0}^{b,b} & \mathrm{W}_{0,0}^{b,c}\\ \mathrm{W}_{0,0}^{c,a} & \mathrm{W}_{0,0}^{c,b} & \mathrm{W}_{0,0}^{c,c}\end{bmatrix}=\widehat{\mathbf{V}}_0\cdot\left(\widehat{\mathbf{V}}_0\right)^H \quad (23j)$$

$$\mathbf{W}_c\succcurlyeq 0;\quad \forall c\in\boldsymbol{\mathcal{C}} \quad (23k)$$

$$r_{n,m}^2\cdot\mathbf{W}_{n,n}=r_{n,m}^2\cdot\begin{bmatrix}\mathrm{W}_{n,n}^{a,a} & \mathrm{W}_{n,n}^{a,b} & \mathrm{W}_{n,n}^{a,c}\\ \mathrm{W}_{n,n}^{b,a} & \mathrm{W}_{n,n}^{b,b} & \mathrm{W}_{n,n}^{b,c}\\ \mathrm{W}_{n,n}^{c,a} & \mathrm{W}_{n,n}^{c,b} & \mathrm{W}_{n,n}^{c,c}\end{bmatrix}=\begin{bmatrix}\mathrm{W}_{m,m}^{a,a} & \mathrm{W}_{m,m}^{a,b} & \mathrm{W}_{m,m}^{a,c}\\ \mathrm{W}_{m,m}^{b,a} & \mathrm{W}_{m,m}^{b,b} & \mathrm{W}_{m,m}^{b,c}\\ \mathrm{W}_{m,m}^{c,a} & \mathrm{W}_{m,m}^{c,b} & \mathrm{W}_{m,m}^{c,c}\end{bmatrix}=\mathbf{W}_{m,m};\quad \forall(n,m)\in\boldsymbol{\mathcal{T}} \quad (23l)$$

$$r_{n,m}^{min}\le r_{n,m}\le r_{n,m}^{max};\quad \forall(n,m)\in\boldsymbol{\mathcal{T}} \quad (23m)$$

Subject to (2)-(3), (5)-(6), (8)-(9), (11), and (13) (23n)

As constraint (23l) is still nonlinear, following the strategy discussed in [19]-[20] to relax (23l)-(23m) as (24), the first chordal relaxation based unbalanced ACOPF model denoted as **CROPF-1** is derived, which includes the objective function (23a) as well as constraints (23b)-(23k), (23n), and (24).

$$\left(r_{n,m}^{min}\right)^2\cdot\mathrm{W}_{n,n}^{\phi,\phi}\le\mathrm{W}_{m,m}^{\phi,\phi}\le\left(r_{n,m}^{max}\right)^2\cdot\mathrm{W}_{n,n}^{\phi,\phi};\ (n,m)\in\boldsymbol{\mathcal{T}} \quad (24)$$

However, solutions to CROPF-1 are rarely exact as will be illustrated in case studies. The main reason is that (24) is not tight enough to describe the relationship between $\mathrm{W}_{n,n}^{\phi,\rho}$ and $\mathrm{W}_{m,m}^{\phi,\rho}$ for $(n,m)\in\boldsymbol{\mathcal{T}}$. Indeed, constraint (23l) shows that the coupling relationship exists not only in diagonal elements, but also in off-diagonal elements. In fact, coupling for diagonal elements only describes the relationship of voltage magnitudes between primary and secondary buses (e.g., $\mathrm{W}_{n,n}^{a,a}$ and $\mathrm{W}_{m,m}^{a,a}$ are squared voltage magnitudes of phase a at primary and secondary buses), while coupling for off-diagonal elements will further ensure that voltage phase angle differences among three phases in both primary and secondary buses are consistent (e.g., $r_{n,m}^2\cdot\mathrm{W}_{n,n}^{b,a}=\mathrm{W}_{m,m}^{b,a}$ represents that voltage phase angle differences between phases a and b at the primary bus n is the same as that of the secondary bus m).

Alternatively, a tighter convexification for (23l)-(23m) is proposed as in (25)-(26). This derives the second chordal relaxation based unbalanced ACOPF model denoted as **CROPF-2**, which includes the objective (23a) as well as constraints (23b)-(23k), (23n), and (25)-(26).

$$\left(r_{n,m}^{max}\right)^2\cdot\mathbf{W}_{n,n}-\mathbf{W}_{m,m}\succcurlyeq 0 \quad (25)$$

$$-\left(r_{n,m}^{min}\right)^2\cdot\mathbf{W}_{n,n}+\mathbf{W}_{m,m}\succcurlyeq 0 \quad (26)$$

Comparing with the original nonlinear and nonconvex ACOPF problem (20), both CROPF-1 and CROPF-2 are convex SDP problems. In turn, they can be solved more efficiently, which also present property that a local optimal solution is also global optimal. Proposition 1 describes the conditions under which the global optimal solution to the original ACOPF model (20) can be retrieved from optimal solutions of CROPF-1/CROPF-2. Proposition 2 further states that the proposed model CROPF-2 is tighter than CROPF-1. Proofs of Propositions 1 and 2 are provided in the Appendix C and D, respectively.

It is worth emphasizing that in terms of the two conditions in Proposition 1, the optimal solution to CROPF-1/CROPF-2 can be directly checked against constraints (23l)-(23m) to see if they are met. On the other hand, the rank one condition may face with numerical issues, as the optimal solution to CROPF-1/CROPF-2 may not be exactly rank-1, in the sense that the second largest eigenvalue may not be strictly zero due to numerical errors. In order to further evaluate the solution accuracy, bus voltages recovered from the solution to $\mathbf{W}_c$ will be used in case studies to calculate system real and reactive power mismatches, which provides another insight on whether the optimal solution to CROPF-1/CROPF-2 is physically feasible to, and in turn global optimal, the original ACOPF problem.

Proposition 1: For an unbalanced radial distribution system, if optimal solutions of $\mathbf{W}_c$ to CROPF-1 or CROPF-2 are rank one and (23l)-(23m) are satisfied, the global optimal solution to the original ACOPF problem (20) can be retrieved from optimal solutions of $\mathbf{W}_c$.

Proposition 2: Any feasible solution to CROPF-2 is also a feasible solution to CROPF-1, and at least one feasible solution to CROPF-1 is infeasible to CROPF-2. That is, (25)-(26) is a tighter relaxation of (23l)-(23m) than (24).

IV. Case Studies

Two systems are studied to illustrate the effectiveness of the proposed chordal relaxation based SDP approach and the tighter convexification formulation (25)-(26) for VRTs.

A. The modified IEEE 34-bus system

The IEEE 34-bus system shown in Fig. 3 includes 34 original buses and two virtual buses 7 and 20 for the two VRTs. Lower and upper bounds on tap ratios of the two VRTs are set as 0.95p.u. and 1.05p.u.. The maximum line current is set as 0.160kA for all lines. A three-phase conventional DER GA is connected at bus 17. Renewable DER GB, is connected

This article has been accepted for publication in a future issue of this journal, but has not been fully edited. Content may change prior to final publication. Citation information: DOI 10.1109/TPWRS.2017.2707564, IEEE Transactions on Power Systems

at bus 30 with η_g of 0.02. The detailed data of GA and GB are provided in Tables I-II, respectively. SVCA is a single phase SVC connected at phase *a* of bus 12, with reactive power limits of [-550kvar, 850kvar]. Three flexible loads are connected at buses 16, 23, and 33, respectively. Data of flexible loads is shown in Table III. Power factor limits of both DERs are set as [0, 1], and those of the three flexible loads are set as [0.85, 1]. A balanced three-phase resistive CIL with 10kW per phase at 1 p.u. voltage level is connected at bus 26. Electricity price c_0 at the distribution substation bus is 10¢/kWh. Distribution substation bus voltages are $1\angle 0^\circ$p.u., $1\angle$-120°p.u., and $1\angle 120^\circ$p.u.. For all other buses, phase voltage magnitude limits are [0.95p.u., 1.05p.u.]. Other configuration data can be found in [27]. Numerical simulations are conducted on a personal computer with Intel Core i7 3.60 GHz processor and 16 GB RAM.

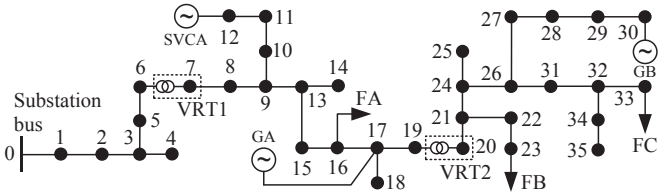

Fig. 3 The modified IEEE 34-bus distribution system with two VRTs

TABLE I
DATA OF THE CONVENTIONAL DER GA

Phase	c_{g2} (×10^{-5}¢/kWh^2)	c_{g1} (¢/kWh)	c_{g0} (¢)	P_g^{max} (kW)	P_g^{min} (kW)	Q_g^{max} (kvar)	Q_g^{min} (kvar)
a	189	6.1	1000	1680	200	720	100
b	203	6.3	1000	1680	200	780	100
c	195	6.0	1000	1680	200	700	100

TABLE II
DATA OF THE RENEWABLE DER GB

Phase	c_{g1} (¢/kWh)	P_g^{max} (kW)	P_g^{min} (kW)	S_g^{max} (kVA)
a	5.1	1250	0	1400
b	5.2	1250	0	1350
c	5.6	1250	0	1350

TABLE III
DATA OF FLEXIBLE LOADS

Flexible load	Phase	b_{d2} (×10^{-5}¢/kWh^2)	b_{d1} (¢/kWh)	b_{d0} (¢)	P_d^{max} (kW)	P_d^{min} (kW)	Q_d^{max} (kvar)	Q_d^{min} (kvar)
	a	-288	10	-200	230	0	120	20
FA	*b*	-578	12.2	-200	230	0	120	20
	c	-592	11.6	-200	230	0	120	20
	a	-255	16.0	-200	1500	0	750	350
FB	*b*	-298	16.7	-200	1500	0	750	350
	c	-243	15.7	-200	1500	0	750	350
	a	-452	12.9	-200	390	0	200	95
FC	*b*	-442	11.4	-200	460	0	220	120
	c	-436	12.3	-200	490	0	250	50

The following four cases are studied. All SDP models are solved by SeDuMi [28].

Case 1: The rank relaxation based SDP model [16].

Case 2: The first chordal relaxation based model CROPF-1.

Case 3: The proposed model CROPF-2.

Case 4: The impact of CILs on the optimal operation of distribution systems.

Case 5: The impact of line current limit on the optimal operation of distribution systems.

Case 1: The rank relaxation based SDP model [16] is first studied to solve the ACOPF problem (20). That is, a single positive semidefinite matrix $\bar{\mathbf{W}}$ for the entire system is built to contain all $W_{n,m}^{\phi,\rho}$ variables, which substitute all $V_n^\phi \cdot \left(V_m^\rho\right)^*$ in $\mathbf{V} \cdot (\mathbf{V})^H$ no matter whether $V_n^\phi \cdot \left(V_m^\rho\right)^*$ appears in (20) or not. The dimension of $\bar{\mathbf{W}}$ is 108×108 and in turn $\bar{\mathbf{W}}$ contains 108^2 $W_{n,m}^{\phi,\rho}$ variables. The ideal transformer constraints (23l)-(23m) are replaced by (24).

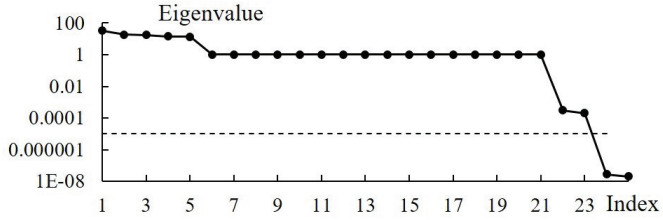

Fig.4 Eigenvalues of matrix $\bar{\mathbf{W}}$

The rank relaxation based SDP model is solved in 2850s. Fig. 4 shows eigenvalues of $\bar{\mathbf{W}}$ on a logarithmic scale. As the rank of a matrix is equal to the number of its nonzero eigenvalues, the threshold of 1×10^{-5} is used to determine whether a numerical eigenvalue solution is nonzero. Fig. 4 shows that 23 eigenvalues are larger than 1×10^{-5}, and in turn the rank of $\bar{\mathbf{W}}$ is 23. Thus, the solution to the rank relaxation based SDP model cannot be used to retrieve a feasible $\mathbf{V}$ solution to the original ACOPF problem (20). The major reason is that $\bar{\mathbf{W}}$ contains high rank sub-matrices $\begin{bmatrix}\mathbf{W}_{n,n} & \mathbf{W}_{n,m}\\ \mathbf{W}_{m,n} & \mathbf{W}_{m,m}\end{bmatrix}$ corresponding to VRTs $(n,m) \in \boldsymbol{\mathcal{T}}$. As $\mathbf{W}_{n,m}$ and $\mathbf{W}_{m,n}$ are not presented in any constraint of the rank relaxation based SDP model, they can take any value as long as $\bar{\mathbf{W}} \succcurlyeq 0$ is met. For instance, if they take values of $\mathbf{0}$, the rank of $\begin{bmatrix}\mathbf{W}_{n,n} & \mathbf{W}_{n,m}\\ \mathbf{W}_{m,n} & \mathbf{W}_{m,m}\end{bmatrix} = \begin{bmatrix}\mathbf{W}_{n,n} & \mathbf{0}\\ \mathbf{0} & \mathbf{W}_{m,m}\end{bmatrix}$ is always no smaller than 2, because $\mathbf{W}_{n,n} \neq \mathbf{0}$ and $\mathbf{W}_{m,m} \neq \mathbf{0}$. That is, as high rank sub-matrices $\begin{bmatrix}\mathbf{W}_{n,n} & \mathbf{W}_{n,m}\\ \mathbf{W}_{m,n} & \mathbf{W}_{m,m}\end{bmatrix}$ are contained in $\bar{\mathbf{W}}$, the rank of $\bar{\mathbf{W}}$ is always no smaller than 2. In turn, in addition to its expensive computational burden, the rank relaxation based SDP model cannot derive feasible $\mathbf{V}$ solutions to the original ACOPF problem (20).

Case 2: In this case, the first chordal relaxation based model CROPF-1 is studied, which includes 33 $\mathbf{W}_c$ corresponding to 33 maximal cliques for all lines. Computational time is 1.2 s, which is about 10^3 times faster than that in Case 1. However, solutions to 20 $\mathbf{W}_c$ matrices corresponding to all 20 lines in the downstream of VRT-1 are of high rank. In fact, VRT-1 partitions the original system into two sub-systems, which are linked by $P_6^\phi = P_7^\phi$, $Q_6^\phi = Q_7^\phi$, and (24). As (24) is not

This article has been accepted for publication in a future issue of this journal, but has not been fully edited. Content may change prior to final publication. Citation information: DOI 10.1109/TPWRS.2017.2707564, IEEE Transactions on Power Systems

binding at the optimal solution to CROPF-1, when fixing P_6^{ϕ}, Q_6^{ϕ}, P_7^{ϕ}, and Q_7^{ϕ} as the optimal solution to CROPF-1, the upstream and downstream sub-systems are decoupled. In turn, three-phase voltage angle differences at bus 7 are not constrained, and the rank of $\mathbf{W}_{7,7}$ is of high order. Similarly, matrices $\mathbf{W}_c$ corresponding to all downstream three-phase lines are of high rank.

In turn, according to Proposition 1, the solution derived from CROPF-1 is infeasible to the original ACOPF problem (20). Indeed, when the rank of $\mathbf{W}_c$ is larger than one, $\mathbf{W}_c$ cannot be directly decomposed as the product of a voltage sub-vector and its conjugate transpose. Although some feasible solution recovery methods [18] may be used to recover a feasible solution around the obtained infeasible solution from CROPF-1, they are based on the condition that the second largest eigenvalue of $\mathbf{W}_c$ should be small enough which indicates that $\mathbf{W}_c$ is close to rank one. However, it is found that this condition is not met in this case. For instance, for certain $\mathbf{W}_c$ solutions in Case 2, the largest eigenvalue is 3.484 and the second largest eigenvalue is 2.598. Thus, feasible solution recovery methods [18], may not work for this case. In addition, solution recovery methods involve an iterative procedure and may require a significant computational time. Consequently, the advantage on computational efficiency of CROPF-1 will be compromised. In summary, this comes to the conclusion that CROPF-1 may be invalid.

Case 3: The proposed chordal relaxation based model CROPF-2 with the tighter convexification formulation (25)-(26) for VRTs is solved. The computational time is 1.3 s. In the optimal solution, all $\mathbf{W}_c$ matrices are rank one and (23l)-(23m) are satisfied. Thus, the optimal solution to the original ACOPF problem can be retrieved according to Proposition 1.

The retrieved three-phase voltage magnitude profiles are shown in Fig. 5. Missing nodes in the profiles represent two-phase and single-phase situations of certain buses. Fig. 5 shows that voltages of all three phases at buses 7 and 20 are boosted by VRT-1 and VRT-2. Table IV shows voltages of primary and secondary buses of the two VRTs, with optimal tap ratios of 1.05p.u. and 1.0306p.u.. Voltage of phase *a* at bus 20 reaches its upper bound. The reason is that a higher voltage will reduce power losses of distribution lines, and in turn the total operation cost can be reduced. Table IV also shows that primary and secondary voltage phase angles for all three phases of VRT-1 and VRT-2 are identical. Thus, (23l)-(23m) are satisfied and the effectiveness of the proposed tighter convexification model (25)-(26) is verified.

In this case, the optimal objective value is 1037.25$, with 350.71$, 338.47$, and 348.67$ for phases *a*, *b*, and *c*, respectively. Real and reactive power outputs of SVC, DERs, and the distribution substation bus are shown in Table V. It shows that as GA's generator in phase *b* and GB's generator in phase *c* are more expensive, they provide less real power than generators in the other phases. Reactive power output of SVCA in phase *a* and three-phase reactive power outputs of GA all reach their upper bounds. Optimal apparent powers through the inverters of GB are 1400kVA, 1350kVA, and 1350kVA in phases *a*, *b*, and *c*, respectively. That is, GB fully utilizes its reactive power capacities. In summary, both SVCA and DERs take full advantage of their reactive power capacities, because more reactive power contributes to higher voltage profiles, reduces system losses, and in turn cuts down the system operation cost.

Optimal operation statuses of the three flexible loads are shown in Table VI. Reactive power dispatches of flexible loads are all at their lower bounds. That is, flexible loads reduce their reactive power consumptions as much as possible, which would help maintain higher voltage profiles and in turn reduce system losses and the system operation cost. Furthermore, phase *a* of FA and phase *b* of FC reach their lower power factor bounds of 0.85. In addition, marginal benefits of these two flexible loads are 9.81¢/kWh and 9.69¢/kWh, which are both smaller than 10¢/kWh of the electricity price at the substation bus. Thus, it indicates that in order to meet power factor limits and minimum reactive power requirements, flexible loads might still consume a certain amount of active power even though the electricity price is higher than their marginal benefits.

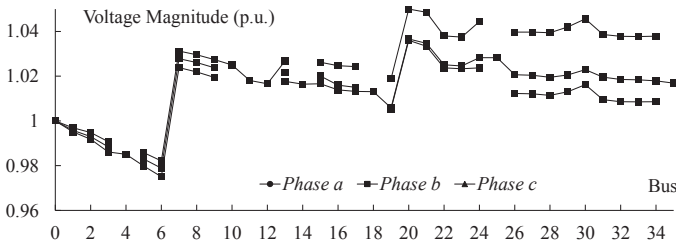

Fig. 5 Three-phase voltage profiles in Case 3

TABLE IV
VOLTAGES OF PRIMARY AND SECONDARY BUSES OF VRTS (P.U.)

Phase	Bus 6	Bus 7	Bus 19	Bus 20
a	0.9821∠-0.49°	1.0312∠-0.49°	1.0189∠0.40°	1.05∠0.40°
b	0.9751∠-120.16°	1.0238∠-120.16°	1.0059∠-120.14°	1.0366∠-120.14°
c	0.9789∠119.95°	1.0278∠119.95°	1.0053∠120.06°	1.0360∠120.06°

TABLE V
REAL AND REACTIVE POWER OUTPUTS OF DERS, SVC, AND THE DISTRIBUTION SUBSTATION BUS

Phase	Substation Bus		SVCA		GA		GB	
	P_0 (kW)	Q_0 (kvar)	P_g (kW)	Q_g (kvar)	P_g (kW)	Q_g (kvar)	P_g (kW)	Q_g (kvar)
a	3449.0	1077.4	-	850	1151.2	720	1250	630.5
b	3409.4	1918.7	-	-	1043.1	780	1250	509.9
c	3249.1	1988.0	-	-	1155.2	700	1250	509.9

TABLE VI
OPTIMAL OPERATION STATUSES OF FLEXIBLE LOADS

Phase	FA			FB			FC		
	P_d (kW)	Q_d (kvar)	Power Factor	P_d (kW)	Q_d (kvar)	Power Factor	P_d (kW)	Q_d (kvar)	Power Factor
a	32.3	20.0	0.85	1040.2	350	0.95	240.9	95	0.93
b	145.1	20.0	0.99	985.9	350	0.94	193.6	120	0.85
c	93.7	20.0	0.98	1001.6	350	0.93	139.8	50	0.94

Summary of Cases 1-3: Table VII summarizes and compares

This article has been accepted for publication in a future issue of this journal, but has not been fully edited. Content may change prior to final publication. Citation information: DOI 10.1109/TPWRS.2017.2707564, IEEE Transactions on Power Systems

the performance of Cases1-3. Among the three models, rank relaxation [16] and CROPF-1 cannot provide solutions that satisfy the rank one condition. On the other hand, CROPF-1 and CROPF-2 present similar computational performance while CPU time of the rank relaxation model is significantly long. The reason is that the dimension of $\bar{\mathbf{W}}$ in the rank relaxation model is 108×108 which includes 108^2 $W_{n,m}^{\phi,\rho}$ variables. In comparison, both CROPF-1 and CROPF-2 include 33 6×6 $\mathbf{W}_c$ matrices and 726 $W_{n,m}^{\phi,\rho}$ variables. The large difference in the number of variables is the major reason that the CPU time of the rank relaxation model is significant.

TABLE VII
SUMMARY OF CASES 1-3

Model	CPU time (Second)	Rank one condition	Number of variable $W_{n,m}^{\phi,\rho}$	Size of the largest positive semidefinite matrix
Rank relaxation [16]	2850	No	11664	108×108
CROPF-1	1.2	No	726	6×6
CROPF-2	1.3	Yes	726	6×6

Case 4: This case investigates the impact of CILs on the optimal operation of distribution systems. In order to better illustrate the effect of different CIL values on optimal setting of tap ratios, voltage lower and upper bounds of all buses are set as 0.9p.u. and 1.1p.u.. Per phase value of the three-phase balanced CIL at bus 26 is gradually increased from 10kW to 150kW. Optimal tap ratios with respect to different CIL values at bus 26 are shown in Table VIII. It is worth mentioning that all solutions in Table VIII satisfy Proposition 1, which can be used to derive global optimal solution to the original ACOPF problem (20).

TABLE VIII
OPTIMAL TAP RATIOS WITH DIFFERENT CIL VALUES

Load (kW per phase)	150	100	60	50	10
VRT-1	1.0362	1.05	1.05	1.05	1.05
VRT-2	0.95	0.95	1.0090	1.05	1.05

Because a CIL's power consumption is proportional to the square of voltage magnitude, a higher voltage would induce a larger real power consumption and in turn a higher system operation cost. That is, the CIL connected at bus 26 will offset economic benefit brought by reduced losses with a high voltage profile. In turn, the system voltage profile needs to be optimally regulated for leveraging reduced losses of distribution lines and increased real power consumptions of CILs. It is observed that with large CIL values in the first two columns of Table VIII, economic benefit from reduced losses by boosting voltage magnitudes of downstream system is smaller than that from reduced power consumption of CIL by decreasing voltage magnitude at bus 26. In turn, VRT-2 steps down voltage magnitude at bus 26 for reducing CIL's real power consumption. Indeed, when the CIL is 150kW per phase, VRT-1 also lowers its tap ratio to further reduce voltage at bus-26 as compared to that with CIL of 100kW. On the other extreme, the last two columns show that when the CIL is small, the two VRTs prefer to step up voltages for reducing power losses and decreasing system cost. While for the CIL of 60kW per phase, VRT-2 optimizes its tap ratio to leverage loss reduction of distribution lines and power consumption increase of the CIL.

Case 5: This case further investigates the impact of line current constraints on the performance of the proposed CROPF-2 model and the optimal operation of distribution systems. In this case, the current limit of line (29,30) is set as 0.020kA and the load connected at bus 30 is removed. Thus, line (29,30) could be potentially congested by the DER GB connecting at its downstream. Two scenarios with and without line current limits are studied. In both scenarios, CROPF-2 is solved in 1.4s and all $\mathbf{W}_c$ are rank one. Thus, in this case study, line congestion does not impact the rank of $\mathbf{W}_c$, and the optimal solution to the original ACOPF problem can be retrieved according to Proposition 1. However, this may not be a general conclusion.

Dispatch results of GB with and without line current constraints are shown in Table IX. It can be seen that, when congestion happens on line (29,30), power generated by GB cannot be fully transmitted through line (29,30) for economically supplying loads, and in turn GB reduces its generation significantly, especially reactive power, even though its marginal cost is lower than that of the main grid. In fact, marginal costs of GB are 5.1¢/kWh, 5.2¢/kWh, and 5.6¢/kWh for phases a, b and c, while electricity price at the substation bus is 10¢/kWh. Consequently, the total system operation cost is increases from 925.21$ to 990.49$ when line current limits are considered.

TABLE IX
DISPATCH OF GB WITH AND WITHOUT LINE CURRENT LIMITATION

Phase	With line current limitation		Without line current limitation	
	P_g (kW)	Q_g (kvar)	P_g (kW)	Q_g (kvar)
a	937.0	103.1	1250	630.5
b	832.2	67.3	1250	509.9
c	904.5	167.8	1250	509.9

B. The IEEE 8500-node distribution system

The modified IEEE 8500-node distribution system [29], which includes three VRTs, five conventional DERs, six flexible loads, and three SVCs, is further studied to test the proposed chordal relaxation based SDP model CROPF-2. Two strategies are applied to preprocess system data for avoiding numerical issues incurred by extreme-short distribution line segments with very large impedance values: (i) line segments shorter than 75 meters are combined with adjacent segments, and (ii) proper voltage and power bases are selected to rescale coefficients of ACOPF constraints. 1150 out of the original 2469 buses are kept after preprocess, which includes 1147 original buses and 3 virtual buses for the three VRTs, In turn, the CROPF-2 model includes 1146 $\mathbf{W}_c$ matrices. The detailed configuration data can be found in [27].

The CROPF-2 model is solved in 23.7 s, which shows that the proposed chordal relaxation based ACOPF model is an efficient tool for designing optimal operation strategies of

This article has been accepted for publication in a future issue of this journal, but has not been fully edited. Content may change prior to final publication. Citation information: DOI 10.1109/TPWRS.2017.2707564, IEEE Transactions on Power Systems

practical large-scale distributions systems. Furthermore, all 1146 $\mathbf{W}_c$ matrices are rank one and (23l)-(23m) are satisfied. Thus, the optimal solution to the original ACOPF problem (20) can be retrieved according to Proposition 1. Table X shows optimal voltages at primary and secondary sides of the three VRTs, in which tap ratios are all equal to their upper bounds of 1.05. In addition, phase angles at primary and secondary sides of all VRTs are identical, which again indicates the tightness of (25)-(26). In addition, the highest voltage value is 1.0493 p.u., occurring at phase *c* of the bus where the single-phase DER GA is connected at, while the lowest voltage value of 0.95. p.u. occurs at phase *c* of the primary side of VRT-1.

TABLE X
VOLTAGES OF VRT CONNECTING BUSES (P.U.)

Phase	VRT-1		VRT-2		VRT-3	
a	0.9592	1.0072	0.9697	1.0182	0.9916	1.0412
	∠-3.21°	∠-3.21°	∠-1.42°	∠-1.42°	∠-4.50°	∠-4.50°
b	0.9535	1.0012	0.9745	1.0232	0.9777	1.0266
	∠-122.77°	∠-122.77°	∠-121.84°	∠-121.84°	∠-123.69°	∠-123.69°
c	0.9593	1.0073	0.9500	0.9975	0.9971	1.0470
	∠117.80°	∠117.80°	∠118.05°	∠118.05°	∠117.38°	∠117.38°

C. Comparison with General NLP Solvers

This section compares computational performance of the proposed approach with general NLP solvers which directly solve the original nonlinear ACOPF problem (20). The results are presented in Tables XI-XII.

When using SeDuMi to solve CROPF-2 of the two systems, the primal-dual gaps are both smaller than 10^{-7}\$, which shows high solution accuracy achieved by the proposed approach. In order to further evaluate the solution accuracy, bus voltages recovered from the solution to $\mathbf{W}_c$ [10] are further used to calculate system real and reactive power mismatches. Real power mismatch ΔP_n^{ϕ} and reactive power mismatch ΔQ_n^{ϕ} of each phase at each bus respectively are calculated as in (27)-(28), where "$\tilde{\cdot}$" indicates recovered voltage values, dispatch solutions of DERs, SVCs/STAECOMs, loads, and substation bus, as well power transmitted through VRTs. System average real and reactive power mismatches per phase per bus are 1.63×10^{-4} kW and 9.19×10^{-5} kvar for the IEEE 34-bus system, and are 5.48×10^{-4} kW and 5.63×10^{-4} kvar for the IEEE 8500-node system. Thus, solution accuracy is considered sufficient from the engineering point of view.

$$\Delta P_n^{\phi} = \left|tr\left(\mathbf{\Phi}_{P,n}^{\phi}\cdot\tilde{\mathbf{V}}\cdot\tilde{\mathbf{V}}^{H}\right) - \left(\sum_{g\in\mathcal{G}_n^{\phi}\cup\mathcal{R}_n^{\phi}}\tilde{P}_g - \sum_{d\in\mathcal{D}_n^{\phi}\cup\mathcal{F}_n^{\phi}}\tilde{P}_d + \Lambda_n\cdot\tilde{P}_n^{\phi}\right)\right| \quad (27)$$

$$\Delta Q_n^{\phi} = \left|tr\left(\mathbf{\Phi}_{Q,n}^{\phi}\cdot\tilde{\mathbf{V}}\cdot\tilde{\mathbf{V}}^{H}\right) - \left(\sum_{g\in\mathcal{G}_n^{\phi}\cup\mathcal{R}_n^{\phi}}\tilde{Q}_g - \sum_{d\in\mathcal{D}_n^{\phi}\cup\mathcal{F}_n^{\phi}}\tilde{Q}_d + \sum_{s\in\mathcal{S}_n^{\phi}}\tilde{Q}_s + \Lambda_n\cdot\tilde{Q}_n^{\phi}\right)\right| \quad (28)$$

A local search NLP solver IPOPT [30] is also tested. Initial phase voltage values of all buses are set as 1∠0°p.u., 1∠-120° p.u., and 1∠120°p.u., respectively. In order to study the impact of initial settings of variables to IPOPT, two cases are performed, in which IPOPT-1 uses 1 as initial tap ratios and IPOPT-2 uses 1.05. Results in Tables XI-XII show that the proposed approach solves ACOPF problems much faster than IPOPT. Specifically, both IPOPT-1 and IPOPT-2 terminate at suboptimal solutions (i.e., 0.063% and 0.110% larger than the solution from the proposed approach). Indeed, in recognizing the facts that the system average real power mismatch is at the level of 10^{-4} kW, the total active power mismatch is less than 1 kW, and the system marginal cost is at the level of 10¢/kWh, difference in the objective value between the proposed approach (i.e., \$989.44) and IPOPT (i.e., \$990.07) can justify that the proposed approach derives a better solution than IPOPT (i.e., difference in the objective value is 63¢ or equivalent about 6.3kW).

Furthermore, tap ratios of VRT-1, VRT-2, and VRT-3 obtained by IPOPT-1 respectively are 1.049, 1.046, and 1.025, are 1.05, 1.05, and 1.0352 from IPOPT-2, while are all 1.05 in the proposed approach. To further illustrate the outperformance of the proposed approach, tap ratios of the three VRTs are fixed as solutions provided by IPOPT-1 (i.e., 1.05, 1.05, and 1.0352) and the CROPF-2 is resolved. The objective is 989.91\$, which is closer to the objective from IPOPT-2 (i.e., \$990.07) and larger than the value obtained by the proposed approach (i.e., \$989.44). It shows that the solutions to tap ratios from the IPOPT are not global optimal, which indicates limitations of local-search NLP solvers in exploring global optimal solutions as well as their dependence on initial settings.

Finally, a global optimization solver LindoGlobal [31] is tested. Since LindoGlobal is a global NLP solver, initial values are not required. The relative gap between lower bound (best possible solution) and upper bound (current best solution) is used as the stopping criterion for LindoGlobal, which is set as 0.1%. After running for more than 3000s, optimality gaps of LindoGlobal are more than 157% for both systems. That is, after 3000s, LindoGlobal cannot even identify feasible solutions for both systems that satisfy the stopping criterion.

In summary, although NLP solvers may be applicable for directly solving (20) to local optimal, identifying global optimal solution is still challenging and could be intractable for even small-scale systems. Indeed, this comparison again shows the motivation and advantage of the proposed chordal relaxation based ACOPF approach. Specifically, the proposed approach not only has strong ability in exploring optimal solution but also presents advantages in computational efficiency and initial guess free.

TABLE XI
COMPARISON IN OBJECTIVE VALUE

Model	Solver	Objective (\$)	
		IEEE 34-bus	IEEE 8500-node
Problem (20)	IPOPT-1	1037.25	990.53
	IPOPT-2	1037.25	990.07
	LindoGlobal	-	-
CROPF-2	SeDuMi	1037.25	989.44

TABLE XII
COMPARISON IN COMPUTATIONAL TIME

Model	Solver	CPU time (Second)	
		IEEE 34-bus	IEEE 8500-node
Problem	IPOPT-1	2.5	65.2

This article has been accepted for publication in a future issue of this journal, but has not been fully edited. Content may change prior to final publication. Citation information: DOI 10.1109/TPWRS.2017.2707564, IEEE Transactions on Power Systems

(20)	IPOPT-2	2.4	108.2
	LindoGlobal	>3000	>3000
CROPF-2	SeDuMi	1.3	23.7

In order to illustrate impacts of the number of DERs on the computational performance and solution quality of the proposed ACOPF approach, the IEEE 8500-node system [27] is further tested with 6 more conventional DERs. The CROPF-2 model is solved in 26.1s, which shows that the number of DERs presents limited impact on the computational time because the number of variables introduced by these additional DERs is relatively small as compared to the total number of variables in $\mathbf{W}_c$. In addition, all 1146 $\mathbf{W}_c$ matrices remain rank one and (23l)-(23m) are also satisfied, which indicates that the number of DERs does not impact the solution quality. Tap ratios of VRT-1, VRT-2, and VRT-3 are 1.05, 1.05, and 1.0454, respectively. Furthermore, in this study an additional single-phase DER connected at phase c of bus 977 makes the phase c voltage value of bus 700 reaching its upper bound, which was 1.0493p.u. without this DER. Thus, power injections of these 6 additional DERs contribute to the raise of bus voltage levels and in turn reduce tap ratios of certain VRTs for mitigating potential violations on voltage upper bounds.

D. Further discussions on the continuous tap ratio modeling

Following the convention of many ACOPF studies, this paper models tap ratios as continuous variables (12), which provides a trade-off between model accuracy and computational efficiency and makes it suitable for real-time ACOPF applications in distribution systems. Continuous tap ratio solutions derived from the proposed model can be rounded up to the closest discrete tap ratio values, in order to recover a practical feasible tap ratio solution. In recognizing that voltage regulators usually have 8, 16, or more tap steps upward and downward, which means 17, 33, or more status with the tap ratio step of 0.00625, 0.003125, or even smaller [20], although the recovered discrete tap ratio values may not be the same as the solution of the discrete tap ratio based model, higher granularity tap ratio steps in practice would make the final roundup tap ratio solutions close to those of the discrete tap ratio based model, and thus acceptable in engineer practice.

In fact, the proposed distribution ACOPF model and solution approach can be extended to consider discrete tap ratios, at the cost of higher computational burden. That is, constraints (23l)-(23m) in the proposed model can be replaced to consider tap ratios as discrete variables, which will derive a mixed-integer SDP (MISDP) problem. The MISDP problem can be solved by the branch-and-bound (BAB) method. The idea is to integrate a branch-and-bound (BAB) framework (such as BNB in Yalmip [32] and SCIP [33]) for handling binary variables, and an SDP solver for solving SDP problems at individual BAB nodes with relaxed integer variables. However, in general, solving large-scale MISDP is still facing with the dilemma of computational inefficiency and/or poor solution quality. Indeed, two main factors would impact computational performance of the MISDP based ACOPF model: 1) the number of ideal transformers and the number of tap positions, i.e., the number of binary variables, which may impact the efficiency of the BAB procedure, and 2) the scale of distribution systems, which would impact computational time of each SDP node in the BAB tree. This is the major reason that the application of the MISDP based ACOPF model for large-scale distribution systems is restricted in practice.

Nevertheless, the following case study is provided to show the impact of the discrete tap ratio model on the computational performance. The MISDP based ACOPF problem is solved by integrating the BAB solver BNB in Yalmip for handling binary variables and Mosek for solving SDP problems at individual BAB nodes, because Yalmip has a well-designed interface with Mosek and Mosek is in general faster than SeDuMi. The modified IEEE 34-bus system and the IEEE 8500-node system are studied. For all voltage regulator transformers, $c_{n,m}$ is set as 0.0125 and $K_{n,m}$ is set as 4. That is, each ideal transformer has 4 steps upward and downward, with each step of 0.0125. In turn, each ideal transformer has 9 statuses. The computational performance is shown in Table XIII. It can be seen that, when considering discrete tap ratios the CPU time for solving the MISDP problem is about 2 orders of magnitude higher than that of the continuous tap ratio model. For larger-scale systems with more VRTs, the computational burden will increase significantly due to the increase of both continuous and binary variables.

TABLE XIII
COMPUTATIONAL PERFORMANCE OF DISCRETE TAP RATIO MODEL

Model		IEEE 34-bus	IEEE 8500-node
Discrete tap ratio	CPU time (Second)	22.17	385.8
	# of SDP nodes searched	123	173
	# of total SDP nodes	289 (9^2)	729 (9^3)
	Objective ($)	1037.31	989.86
	Tap ratios	1.05/1.025	1.05/1.05/1.05
Continuous tap ratio	CPU time (Second)	0.21	2.89
	Objective ($)	1037.00	989.86
	Tap ratios	1.05/1.0306	1.05/1.05/1.05

Based on the above study, considering tap radios as continuous variables actually provide significant computational benefits at the cost of accurate tap ratio solutions. Indeed, considering tap radios as continuous variables is consistent with existing studies on transmission and distribution ACOPF problems [R.34]-[R.35], [20], which provides a trade-off between model accuracy and computational efficiency and makes it suitable for real-time ACOPF applications in distribution systems.

V. CONCLUSION

Although network topology of an unbalanced three-phase distribution system is radial, the graph of the unbalanced ACOPF problem is strongly meshed, and in turn ACOPF approaches and conclusions for balanced distribution systems in literature may not be applicable. This paper proposes a chordal relaxation based SDP approach to derive global optimal solutions to unbalanced ACOPF problems. The

This article has been accepted for publication in a future issue of this journal, but has not been fully edited. Content may change prior to final publication. Citation information: DOI 10.1109/TPWRS.2017.2707564, IEEE Transactions on Power Systems

proposed unbalanced ACOPF model determines the optimal operation of conventional DERs, inverter interfaced renewable DERs, and voltage regulation devices for minimizing system operation cost while satisfying prevailing constraints. In addition, a tighter convexification model for VRTs is introduced to mitigate solution inexactness. Analytical conditions are presented and proved to determine whether the global optimal solution to the original ACOPF problem can be retrieved via solutions of the chordal relaxation based SDP model. Numerical case studies show that the proposed chordal relaxation based approach can solve unbalanced ACOPF problems much faster than the rank relaxation based SDP based model and general NLP solvers, and in turn presents a suitable tool for designing optimal operation strategies of practical large-scale distributions systems.

APPENDIX

A An Illustration Example for the Graph of ACOPF

A 4-bus system shown on top of Fig. 6 is used for illustrating how to map the proposed ACOPF problem into a graph. Specifically, the distribution line connecting buses 0-1 is a three-phase line segment, while those connecting buses 1-2 and buses 2-3 respectively are two-phase and single-phase line segments. When mapping the ACOPF problem into a graph as shown on bottom of Fig. 6, voltage variables of individual phases at each bus are represented as nodes, and two nodes V_n^{ϕ} and V_m^{ρ} are connected via an edge if and only if $V_n^{\phi} \cdot \left(V_m^{\rho}\right)^*$ for $n \neq m$ and/or $\phi \neq \rho$ is involved in problem (20). It is worth mentioning that in problem (20), only constraints (17)-(18) and (20c) contain bilinear terms $V_n^{\phi} \cdot \left(V_m^{\rho}\right)^*$ for $n \neq m$ and/or $\phi \neq \rho$.

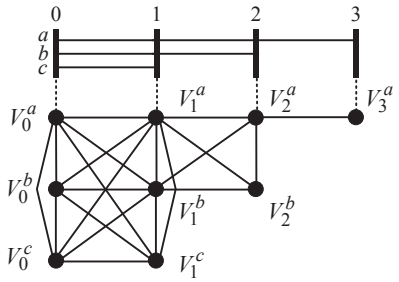

Fig. 6 A 4-bus system and the graph of its ACOPF problem

The graph in Fig. 6 shows that, for instance, $V_0^a - V_1^a - V_1^b - V_0^b - V_0^a$ and $V_0^a - V_1^a - V_1^b - V_0^a$ are both cycles while $V_0^a - V_1^a - V_1^b - V_0^a$ is a minimal cycle. Indeed, it can be seen from Fig. 6 that all minimal cycles exclusively contain three nodes, which means that the graph is chordal. Furthermore, the graph includes three maximal cliques according to the definition of maximal clique in Section III.A, including $\{V_0^a, V_1^a, V_1^b, V_1^c, V_0^c, V_0^b\}$, $\{V_1^a, V_2^a, V_2^b, V_1^b\}$, and $\{V_2^a, V_3^a\}$ which respectively are maximal 6-clique, 4-clique, and 2-clique. Obviously, they are all complete subgraphs and not contained in any other cliques, which means they are all maximal cliques.

Three observations can be made from the graph of the 4-bus example: (i) the graph of the ACOPF problem is constructed by connecting a series of subgraphs in Fig. 2 according to network topology of the distribution system; (ii) subgraphs in Fig. 2 are all maximal cliques; and (iii) each distribution line corresponds to a subgraph in Fig. 2. The graph of the ACOPF problem for more complicated large-scale distribution systems can be similarly constructed by connecting sub-structures in Fig. 2 successively according to the distribution network topology.

B An Illustration Example for Chordal Relaxation

A 4-bus illustrative example with 3 three-phase lines shown in Fig. 7 is used to demonstrate the validity of the chordal relaxation, which separates the **W** matrix into several sub-matrices $\mathbf{W}_c$.

The voltage vector **V** is written as in (29). By introducing new variables $\mathrm{W}_{n,m}^{\phi,\rho}$ to substitute nonlinear terms $V_n^{\phi} \cdot \left(V_m^{\rho}\right)^*$, a 12×12 square matrix **W** can be obtained as in (30). It is noted that as certain nonlinear terms (e.g., $V_0^a \cdot (V_2^a)^*$) do not appear in the ACOPF problem (20), corresponding variable substitutions $\mathrm{W}_{n,m}^{\phi,\rho}$ (e.g., $\mathrm{W}_{0,2}^{a,a}$) are not needed and can be replaced with 0 in order to reduce the number of variables. The corresponding graph is shown in Fig. 8. For the sake of illustration, each of the three nodes in the graph corresponding to V_1^a, V_1^b, and V_1^c is duplicated three times, which are connected via dash lines to indicate that they are the same node. Fig. 8 includes three maximal 6-cliques shown in the three dashed boxes, which correspond to three 6×6 submatrices as in (31). It can be seen that the three $\mathbf{W}_c$ are sub-matrices of **W**, which correspond to sub-vectors of **V** that are contained in each maximal clique of the graph.

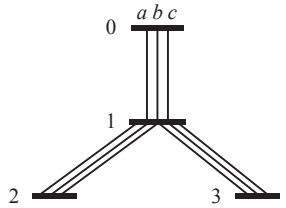

Fig. 7 A 4-bus illustrative example

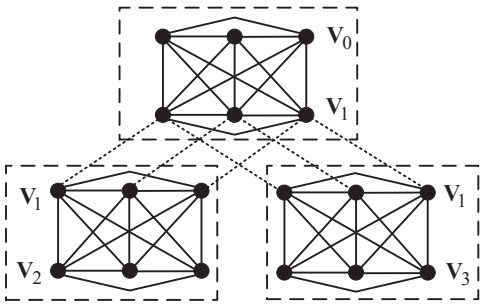

Fig. 8 Graph representation of the ACOPF problem for the 4-bus system

In comparison, the rank relaxation based SDP model [16] is studied in Case 1, in which a 12×12 full square matrix $\overline{\mathbf{W}}$ as shown in (32) is used. That is, a single positive semidefinite

This article has been accepted for publication in a future issue of this journal, but has not been fully edited. Content may change prior to final publication. Citation information: DOI 10.1109/TPWRS.2017.2707564, IEEE Transactions on Power Systems

matrix $\overline{\mathbf{W}}$ for the entire system is built to contain all $\mathrm{W}_{n,m}^{\phi,\rho}$ variables, which substitute all $V_n^{\phi}\cdot(V_m^{\rho})^*$ in $\mathbf{V}\cdot(\mathbf{V})^H$ no matter whether $V_n^{\phi}\cdot(V_m^{\rho})^*$ appears in (20) or not.

$$\mathbf{V}=[\mathbf{V}_0^T\ \mathbf{V}_1^T\ \mathbf{V}_2^T\ \mathbf{V}_3^T]^T \tag{29}$$

$$\mathbf{V}\cdot\mathbf{V}^H=\begin{bmatrix}\mathbf{V}_0\\ \mathbf{V}_1\\ \mathbf{V}_2\\ \mathbf{V}_3\end{bmatrix}\cdot\begin{bmatrix}\mathbf{V}_0\\ \mathbf{V}_1\\ \mathbf{V}_2\\ \mathbf{V}_3\end{bmatrix}^H\Rightarrow\begin{bmatrix}\mathbf{W}_{0,0} & \mathbf{W}_{0,1} & \mathbf{0} & \mathbf{0}\\ \mathbf{W}_{1,0} & \mathbf{W}_{1,1} & \mathbf{W}_{1,2} & \mathbf{W}_{1,3}\\ \mathbf{0} & \mathbf{W}_{2,1} & \mathbf{W}_{2,2} & \mathbf{0}\\ \mathbf{0} & \mathbf{W}_{3,1} & \mathbf{0} & \mathbf{W}_{3,3}\end{bmatrix}=\mathbf{W} \tag{30}$$

$$\begin{bmatrix}\mathbf{V}_0\\ \mathbf{V}_1\end{bmatrix}\cdot\begin{bmatrix}\mathbf{V}_0\\ \mathbf{V}_1\end{bmatrix}^H\Rightarrow\begin{bmatrix}\mathbf{W}_{0,0} & \mathbf{W}_{0,1}\\ \mathbf{W}_{1,0} & \mathbf{W}_{1,1}\end{bmatrix};\begin{bmatrix}\mathbf{V}_1\\ \mathbf{V}_2\end{bmatrix}\cdot\begin{bmatrix}\mathbf{V}_1\\ \mathbf{V}_2\end{bmatrix}^H\Rightarrow\begin{bmatrix}\mathbf{W}_{1,1} & \mathbf{W}_{1,2}\\ \mathbf{W}_{2,1} & \mathbf{W}_{2,2}\end{bmatrix}$$
$$\begin{bmatrix}\mathbf{V}_1\\ \mathbf{V}_3\end{bmatrix}\cdot\begin{bmatrix}\mathbf{V}_1\\ \mathbf{V}_3\end{bmatrix}^H\Rightarrow\begin{bmatrix}\mathbf{W}_{1,1} & \mathbf{W}_{1,3}\\ \mathbf{W}_{3,1} & \mathbf{W}_{3,3}\end{bmatrix} \tag{31}$$

$$\overline{\mathbf{W}}=\begin{bmatrix}\mathbf{W}_{0,0} & \mathbf{W}_{0,1} & \mathbf{W}_{0,2} & \mathbf{W}_{0,3}\\ \mathbf{W}_{1,0} & \mathbf{W}_{1,1} & \mathbf{W}_{1,2} & \mathbf{W}_{1,3}\\ \mathbf{W}_{2,0} & \mathbf{W}_{2,1} & \mathbf{W}_{2,2} & \mathbf{W}_{2,3}\\ \mathbf{W}_{3,0} & \mathbf{W}_{3,1} & \mathbf{W}_{3,2} & \mathbf{W}_{3,3}\end{bmatrix} \tag{32}$$

C Proof for Proposition 1

As CROPF-1 and CROPF-2 are convex SDP problems, a local optimal solution $\mathbf{W}_c$ is also global optimal. In addition, as they are convex relaxations to the original ACOPF (20), their feasible regions are larger than that of (20). In turn, if a feasible $\mathbf{V}$ solution to the original ACOPF problem (20) can be recovered from the optimal solution $\mathbf{W}_c$ to CROPF-1/CROPF-2, it must also be a global optimal solution to (20).

Next, we discuss how to recover a feasible $\mathbf{V}$ solution to (20) from the optimal solution $\mathbf{W}_c$ of CROPF-1/CROPF-2. Without loss of generality, assuming that the distribution substation bus (indexed as 0) is connected to bus 1.

1) As $\begin{bmatrix}\mathbf{W}_{0,0} & \mathbf{W}_{0,1}\\ \mathbf{W}_{1,0} & \mathbf{W}_{1,1}\end{bmatrix}$ is rank one, $\mathbf{W}_{0,1}$ is also rank one. With a given $[\hat{V}_0^a\ \hat{V}_0^b\ \hat{V}_0^c]$ at the distribution substation, voltages of bus 1 can be calculated via $[\hat{V}_0^a\ \hat{V}_0^b\ \hat{V}_0^c]\cdot[V_1^a\ V_1^b\ V_1^c]^H=\mathbf{W}_{0,1}$;

2) Voltages of remaining buses can be successively retrieved according to the network topology. With retrieved voltages $[\hat{V}_n^a\ \hat{V}_n^b\ \hat{V}_n^c]$ for bus n,

a) If bus m is connected to bus n via a distribution line, voltages of bus m can be retrieved via $[\hat{V}_n^a\ \hat{V}_n^b\ \hat{V}_n^c]\cdot[V_m^a\ V_m^b\ V_m^c]^H=\mathbf{W}_{n,m}$, as $\begin{bmatrix}\mathbf{W}_{n,n} & \mathbf{W}_{n,m}\\ \mathbf{W}_{m,n} & \mathbf{W}_{m,m}\end{bmatrix}$ is rank one;

b) If bus m is connected to bus n via a VRT, voltages of bus m can be obtained via $[V_m^a\ V_m^b\ V_m^c]=\hat{r}_{n,m}\cdot[\hat{V}_n^a\ \hat{V}_n^b\ \hat{V}_n^c]$, as (23l)-(23m) are met and a unique $\hat{r}_{n,m}$ is determined.

In summary, a feasible $\mathbf{V}$ solution to the original problem, thereby global optimal to (20), can be retrieved from the optimal solution $\mathbf{W}_c$ to CROPF-1/ CROPF-2 under the conditions that all $\mathbf{W}_c$ are rank one and (23l)-(23m) are met.

D Proof for Proposition 2

We first prove that any feasible solution to CROPF-2 is also feasible to CROPF-1. If a feasible solution to CROPF-2 does not satisfy (24), without loss of generality, we consider the upper bound being violated, i.e., $\mathrm{W}_{m,m}^{\phi,\phi}>\left(r_{n,m}^{max}\right)^2\cdot\mathrm{W}_{n,n}^{\phi,\phi}$. That is, diagonal elements of $\left[\left(r_{n,m}^{max}\right)^2\cdot\mathbf{W}_{n,n}-\mathbf{W}_{m,m}\right]$ are all negative. This is contrary to the assumption that it is a feasible solution to CROPF-2 as the positive semidefinite constraint (25) is violated. Thus, a feasible solution to CROPF-2 always satisfies (24), and in turn is feasible to CROPF-1.

To prove the second part, a branch in Fig. 9 is considered as an example. With a feasible solution $\widehat{\mathbf{W}}_{n,n}$ to CROPF-1 together with $\hat{P}_n^{\phi}$, $\hat{P}_m^{\phi}$, $\hat{Q}_n^{\phi}$, and $\hat{Q}_m^{\phi}$, if a fixed load at bus $(m+1)$ satisfies $P_{f,m+1}^{\phi}=-tr\left(\mathbf{\Phi}_{P,m+1}^{\phi}\cdot\widehat{\mathbf{W}}\right)$ and $Q_{f,m+1}^{\phi}=-tr\left(\mathbf{\Phi}_{Q,m+1}^{\phi}\cdot\widehat{\mathbf{W}}\right)$ while (23l) and (24) are also met, $\widehat{\mathbf{W}}_{m,m}=\left(r_{n,m}^{max}\right)^2\cdot diag\left(\widehat{\mathbf{W}}_{n,n}\right)$ is a feasible solution for bus m. Thus, $\left[\left(r_{n,m}^{max}\right)^2\cdot\widehat{\mathbf{W}}_{n,n}-\widehat{\mathbf{W}}_{m,m}\right]=\begin{bmatrix}0 & \widehat{\mathrm{W}}_{n,n}^{a,b} & \widehat{\mathrm{W}}_{n,n}^{a,c}\\ \widehat{\mathrm{W}}_{n,n}^{b,a} & 0 & \widehat{\mathrm{W}}_{n,n}^{b,c}\\ \widehat{\mathrm{W}}_{n,n}^{c,a} & \widehat{\mathrm{W}}_{n,n}^{c,b} & 0\end{bmatrix}$. Because determinant $\left|\begin{bmatrix}0 & \widehat{\mathrm{W}}_{n,n}^{a,b}\\ \widehat{\mathrm{W}}_{n,n}^{b,a} & 0\end{bmatrix}\right|=-\widehat{\mathrm{W}}_{n,n}^{a,b}\cdot\widehat{\mathrm{W}}_{n,n}^{b,a}=-\left(\widehat{\mathrm{W}}_{n,n}^{b,a}\right)^H\cdot\widehat{\mathrm{W}}_{n,n}^{b,a}=-\left|\widehat{\mathrm{W}}_{n,n}^{b,a}\right|^2<0$, $\left[\left(r_{n,m}^{max}\right)^2\cdot\widehat{\mathbf{W}}_{n,n}-\widehat{\mathbf{W}}_{m,m}\right]$ is negative semidefinite and (25) is violated. That is, a feasible solution to CROPF-1 could be infeasible to CROPF-2.

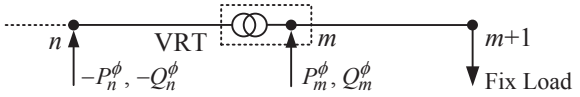

Fig. 9 An illustrative example with a VRT and a fixed load

REFERENCES

[1] A. Keane, L.N.O. Ochoa, E. Vittal, C.J. Dent, and G.P. Harrison, "Enhanced utilization of voltage control resources with distributed generation," *IEEE Trans. Power Syst*., vol. 26, no. 1, pp. 252-260, May 2011.

[2] National Academies of Sciences, Engineering, and Medicine, Analytic research foundations for the next-generation electric grid, Washington DC, USA: National Academic Press 2016.

[3] X. Bai, H. Wei, K. Fujisawa, and Y. Wang, "Semidefinite programming for optimal power flow problems," *Int. J. Elect. Power Energy Syst*., vol. 30, no. 6-7, pp. 383-392, 2008.

[4] J. Lavaei and S.H. Low, "Zero duality gap in optimal power flow problem," *IEEE Trans. Power Syst*., vol. 27, no. 1, pp. 92-106, Feb. 2012.

[5] S.H. Low, "Convex relaxation of optimal power flow -- part I: formulation and equivalence," *IEEE Trans. Control Network Syst*., vol. 1, no. 1, pp. 15-27, Mar. 2014.

[6] R.A. Jabr, "Exploiting sparsity in SDP relaxations of the OPF problem," *IEEE Trans. Power Syst*., vol. 27, no. 2, pp. 1138-1139, May 2012.

[7] M.S. Andersen, A. Hansson, and L. Vandenberghe, "Reduced-complexity semidefinite relaxations of optimal power flow problems," *IEEE Trans. Power Syst.*, vol. 29, no. 4, pp. 1855-1863, Jul. 2014.

[8] D.K. Molzahn, J. Holzer, B. Lesieutre, and C. DeMarco, "Implementation of a large-scale optimal power flow solver based on semidefinite programming," *IEEE Trans. Power Syst*., vol. 28, no. 4, pp. 3987-3998, Nov. 2013.

[9] B. Ghaddar, J. Marecek, and M. Mevissen "Optimal Power Flow as a Polynomial Optimization Problem", *IEEE Trans. Power Syst*., vol. 31, no. 1, pp. 539-546, Jan 2016.

[10] D.K. Molzahn and I.A. Hiskens, "Sparsity-Exploiting Moment-Based Relaxations of the Optimal Power Flow Problem," *IEEE Trans. Power Syst*., vol.30, no. 6, pp.3168-3180, Nov. 2015.

[11] R.A. Jabr, "Radial distribution load flow using conic programming," *IEEE Trans. Power Syst.*, vol. 21, no. 3, pp. 1458-1459, Aug. 2006.
[12] R.A. Jabr, "A conic quadratic format for the load flow equations of meshed networks," *IEEE Trans. Power Syst.*, vol. 22, no. 4, pp. 2285-2286, Nov. 2007.
[13] M. Farivar and S.H. Low, "Branch flow model: relaxations and convexification - part I," *IEEE Trans. Power Syst.*, vol. 28, no. 3, pp. 2554-2564, Aug. 2013.
[14] S. Bose, D. Gayme, and S. Low, "Optimal power flow over tree networks," *49th Annual Allerton Conference on Communication, Control, and Computing* (*Allerton*), Sep. 2011.
[15] B. Zhang and D. Tse, "Geometry of injection regions of power networks," *IEEE Trans. Power Syst.*, vol. 28, no. 2, pp. 788-796, May 2013.
[16] E.D. Anese, H. Zhu, and G.B. Giannakis, "Distributed optimal power flow for smart microgrids," *IEEE Trans. Smart Grid*, vol. 4, no. 3, pp. 1464-1475, Sep. 2013.
[17] Q. Peng and S.H. Low, "Distributed algorithm for optimal power flow on unbalanced multiphase distributed networks," arXiv: 1512.06482v1, Dec. 2015.
[18] Y. Liu, J. Li, and L. Wu, "Distribution system restructuring: distribution LMP via Unbalanced ACOPF," *IEEE Trans*. *Smart Grid*, DOI: 10.1109/TSG.2016.2647692, 2017.
[19] B.A. Robbins, H. Zhu, and A.D. Dominguez-Gracia, "Optimal tap setting of voltage regulation transformers in unbalanced distribution networks," *2013 North American Power Symposium. (NAPS)*, Sep. 2013.
[20] B.A. Robbins, H. Zhu, and A.D. Dominguez-Gracia, "Optimal tap setting of voltage regulation transformers in unbalanced distribution systems," *IEEE Trans. Power Syst.*, vol. 31, no. 1, pp. 256-267, Jan. 2016.
[21] S. Bose, S. Low, T. Teeraratkul, and B. Hassibi, "Equivalent relaxations of optimal power flow," *IEEE Trans. Autom. Control*, vol. 60, no. 3, pp. 729-742, Mar. 2015.
[22] P.B.S. Kiran and N.M. Pindoriya "Study of consumer benefit functions for demand response algorithm," 2016 *National Power Systems Conference (NPSC)*, Dec. 2016.
[23] M. O'boyle, "Who should own and operate distributed energy resources?" [Online]. Available: http://docplayer.net/14659309-Who-should-own-and-operate-distributed-energy-resources.html. Accessed: February 25, 2017.
[24] J.D. Glover, M.S. Sarma, and T.J. Overbye, Power System Analysis and Design, Stamford, CT, USA: Cengage Learning, 2010.
[25] S. Sojoudi and J. Lavaei, "Exactness of semidefinite relaxations for nonlinear optimization problems with underlying graph structure," *SIAM Journal on Optimization*, vol. 24, pp. 1746-1778, 2015.
[26] S.H. Low, "Convex relaxation of optimal power flow -- part II: Exactness," *IEEE Trans. Control Network Syst*., vol. 1, no. 2, pp. 177-189, Jun. 2014.
[27] http://www.clarkson.edu/~lwu/data/ChordalACOPF/. Accessed: February 19, 2017.
[28] SeDuMi, http://sedumi.ie.lehigh.edu/. Accessed: February 19, 2017.
[29] IEEE 8500-node system, http://ewh.ieee.org/soc/pes/dsacom/testfeeders. Accessed: February 19, 2017.
[30] IPOPT, https://projects.coin-or.org/Ipopt. Accessed: February 19, 2017.
[31] LindoGlobal, http://www.lindo.com/. Accessed: February 19, 2017.
[32] Yalmip, https://yalmip.github.io/. Accessed: February 28, 2017.
[33] SCIP, http://scip.zib.de/. Accessed: February 28, 2017.

BIOGRAPHIES

Yikui Liu (S'15) received the B.S. degree in electrical engineering and automation from Nanjing Institute of Technology, China, in 2012 and the M.S. degree in power system and automation from Sichuan University, China, in 2015. He is currently pursuing the Ph.D. degree with Electrical and Computer Engineering Department, Clarkson University, USA. His current research interests are power market and OPF in distribution system.

Jie Li (M'14) received the B.S. degree in information engineering from Xi'an Jiaotong University in 2003 and the M.S. degree in system engineering from Xi'an Jiaotong University, China in 2006, and the Ph.D. degree from the Illinois Institute of Technology (IIT), Chicago, in 2012. From 2006 to 2008, she was a Research Engineer with IBM China Research Lab. From 2012 to 2013, she was a Power System Application Engineer with GE Energy Consulting. Presently, she is an Assistant Professor in the Electrical and Computer Engineering Department at Clarkson University. Her research interests include power systems restructuring and bidding strategy.

Lei Wu (SM'13) received the B.S. degree in electrical engineering and the M.S. degree in systems engineering from Xi'an Jiaotong University, Xi'an, China, in 2001 and 2004, respectively, and the Ph.D. degree in electrical engineering from Illinois Institute of Technology (IIT), Chicago, IL, USA, in 2008. From 2008 to 2010, he was a Senior Research Associate with the Robert W. Galvin Center for Electricity Innovation, IIT. He worked as summer Visiting Faculty at NYISO in 2012. Currently, he is an Associate Professor with the Electrical and Computer Engineering Department, Clarkson University, Potsdam, NY, USA. His research interests include power systems operation and planning, energy economics, and community resilience microgrid.

Tom Ortmeyer (F'03) is a Professor of Electrical and Computer Engineering (ECE) at Clarkson University. Dr. Ortmeyer has research interests in power quality, power distribution, power electronics, distributed and renewable energy resources, and power system protection. He directed the Alcoa Experiential Learning Program, and was ECE Department Chair from 2001–2010.